



1

2

3 **Estimating nitrogen and sulfur deposition across China**
4 **during 2005-2020 based on multiple statistical models**

5

6 Kaiyue Zhou¹, Wen Xu³, Lin Zhang⁴, Mingrui Ma¹, Xuejun Liu³, Yu Zhao^{1,2*}

7

8 1. State Key Laboratory of Pollution Control & Resource Reuse and School of the
9 Environment, Nanjing University, Nanjing, Jiangsu 210023, China

10 2. Jiangsu Collaborative Innovation Center of Atmospheric Environment and
11 Equipment Technology (CICAEET), Nanjing University of Information Science &
12 Technology, Nanjing, Jiangsu 210044, China

13 3. Key Laboratory of Plant-Soil Interactions of MOE, College of Resources and
14 Environmental Sciences, National Academy of Agriculture Green Development, China
15 Agricultural University, Beijing 100193, China

16 4. Laboratory for Climate and Ocean-Atmosphere Sciences, Department of
17 Atmospheric and Oceanic Sciences, School of Physics, Peking University, Beijing
18 100871, China

19

20 *Corresponding author: Yu Zhao

21 Phone: 86-25-89680650; email: yuzhao@nju.edu.cn

22



23 **Abstract**

24 Due to the rapid development of industrialization and substantial economy, China
25 has become one of the global hotspots of nitrogen (N) and sulfur (S) deposition
26 following Europe and the USA. Here, we developed a dataset with full coverage of N
27 and S deposition from 2005 to 2020, with multiple statistical models that combine
28 ground-level observations, chemistry transport simulations, satellite-derived vertical
29 columns, and meteorological and geographic variables. Based on the newly developed
30 random forest method, the multi-year averages of dry deposition of OXN, RDN and S
31 in China were estimated at 10.4, 14.4 and 16.7 kg N/S ha⁻¹ yr⁻¹, and the analogous
32 numbers for total deposition were respectively 15.2, 20.2 and 25.9 kg N/S ha⁻¹ yr⁻¹
33 when wet deposition estimated previously with a GAM model was included. The
34 $R_{\text{dry/wet}}$ of N stabilized in earlier years and then gradually increased especially for RDN,
35 while that of S declined for over ten years and then slightly increased. $R_{\text{RDN/OXN}}$ was
36 estimated to be larger than 1 for the whole research period and clearly larger than that
37 of the USA and Europe, with a continuous decline from 2005 to 2011 and a more
38 prominent rebound afterwards. Compared with the USA and Europe, a more prominent
39 lagging response of OXN and S deposition to precursor emission abatement was found
40 in China. The OXN dry deposition presented a descending gradient from east to west,
41 while the S dry deposition a descending gradient from north to south. After 2012, the
42 OXN and S deposition in eastern China declined faster than the west, attributable to
43 stricter emission controls. Positive correlation was found between regional deposition
44 and emissions, while smaller deposition to emission ratios (D/E) existed in developed
45 eastern China with more intensive human activities.

46 **1. Introduction**

47 Atmospheric deposition of nitrogen (N) and sulfur (S) is considered as a serious
48 environmental problem, leading to widespread ecosystem acidification and
49 eutrophication, as well as human health damages (Baker et al., 1991; Burns et al., 2016;



50 Payne et al., 2011; Reuss et al., 1987; Zhang et al., 2018a). In order to understand the
51 spatial distribution and temporal variability of deposition, long-term observation
52 networks have been established globally particularly in developed countries or regions,
53 such as Clean Air Status and Trends Network/the National Atmospheric Deposition
54 Program (CASTNET/NADP) in the USA (Beachley et al., 2016), Canadian Air and
55 Precipitation Monitoring Network (CAPMoN) in Canada (Cheng et al., 2022),
56 European Monitoring and Evaluation Program (EMEP) in Europe (Simpson et al.,
57 2012), and Acid Deposit Monitoring Network in East Asia (EANET; Tørseth et al.,
58 2012; Totsuka et al., 2005; Yamaga et al., 2021). Reductions of anthropogenic NO_x and
59 SO₂ emissions in North America have been very effective in reducing the oxidized
60 nitrogen (OXN) and wet S deposition (Cheng and Zhang, 2017; Feng et al., 2021;
61 Likens et al., 2021). In the USA, for example, OXN decreased significantly in most
62 areas, while reduced nitrogen (RDN) increased gradually in agricultural areas (Holland
63 et al., 2005; Li et al., 2016). Similarly, the long-term observation in Europe shows a
64 downward trend for N and S deposition over the last two decades (Keresztesi et al.,
65 2019; Theobald et al., 2019).

66 China has become one of global hotspots of atmospheric deposition due mainly to
67 the large anthropogenic emissions from increased industrial economy and energy
68 consumption for the past two decades (Vet et al., 2014). To reduce soil acidification
69 and improve air quality, the Chinese government has enacted a series of policies to cut
70 the emissions of atmospheric deposition precursors since 2005 (Li et al., 2017; Liu et
71 al., 2015; Zheng et al., 2018a), including the policy of limiting national total emission
72 levels of SO₂ and NO_x within the 11th Five-year Plan (FYP) period (2005-2010), the
73 National Action Plan on the Prevention and Control of Air Pollution (NAPPCAP,
74 2013-2017), and the Three-Year Action Plan to fight air pollution (TYAPFAP,
75 2018-2020). Estimated by the Multiple-resolution Emission Inventory for China
76 (MEIC, <http://www.meicmodel.org>), those policies have reduced annual SO₂ and NO_x
77 emissions from different years (Li, 2020; Wang et al., 2022; Zhang et al., 2019), while



78 the change in NH_3 was relatively small. The SO_2 and NO_x vertical column densities
79 (VCDs) measured from satellite remote sensing have also declined to varying degrees
80 across the country (Krotkov et al., 2016; Xia et al., 2016). Besides emissions and
81 ambient columns, accurate estimation on the changing N and S deposition is crucial for
82 evaluating the effectiveness of national policies on decreasing the ecological risk.
83 Limited by data and methods (explained below), however, few studies have been
84 conducted to link the long-term trend of deposition to the regulations of air pollution
85 prevention.

86 Similar to developed countries, the direct knowledge of deposition in China came
87 first from ground observation. Since 1990s, atmospheric deposition monitoring
88 networks in China have been gradually established and improved, such as the Chinese
89 Nationwide Nitrogen Deposition Monitoring Network (NNDMN; Xu et al., 2019) and
90 the Chinese Ecosystem Research Network (CERN; Fu et al., 2010). They provide
91 essential information for quantifying dry and wet deposition and revealing its
92 long-term variability at site level. For example, Liu et al. (2013) found a significant
93 growth in bulk nitrogen deposition in China between 1980 and 2010 based on
94 meta-analyses of historical observation data. Due to insufficient spatial and temporal
95 coverage, however, data obtained at individual sites could not fully support the analysis
96 of widespread and long-term evolution of deposition and might miss diverse patterns
97 of changing deposition by region (Hou et al., 2019; Lye and Tian, 2007). Statistical
98 methods, which incorporated meteorological and environmental variables with higher
99 temporal and horizontal resolutions and wide coverage in time and space (e.g.,
100 satellite-derived VCDs), have been increasingly applied to fill the observation gap.
101 Linear or nonlinear relationship between those variables and observed deposition have
102 been developed and applied for periods and regions without observation (Jia et al.,
103 2016; Xu et al., 2018; Yu et al., 2019). For example, Liu et al. (2017a) and Zhang et al.
104 (2018b) obtained the removal rate of SO_2 and NO_x by precipitation in the whole
105 atmospheric boundary layer through linear regression method, and estimated the wet S



106 deposition in 2005-2016 and nitrogen in 2010-2012 in China. Relatively high
107 uncertainty existed in the simple linear assumption, given the complicated effects of
108 multiple variables (e.g., meteorological conditions and underlying surface types) on
109 deposition. Although advanced statistical methods such as k-Nearest Neighbor (KNN),
110 Gradient Boosting Machine (GBM) and neural networks have been developed to
111 predict the air pollutant concentrations, they are much rarely used in the estimation of
112 deposition (Li et al., 2020b; Li et al., 2019; Qin et al., 2020; Wu et al., 2021). Out of
113 the limited studies, Li et al. (2020a) developed machine learning prediction methods
114 based on multi-sites observation data and integrated meteorological and land use type
115 information, which improved the prediction accuracy of temporal and spatial
116 distribution of ammonium wet deposition.

117 Besides spatiotemporal coverage, integrated estimation for multiple species is
118 another great challenge, particularly for dry deposition. Compared with wet or bulk
119 deposition, there are very few data available for direct observation of dry deposition
120 and an “inferential method” that incorporates numerical-simulated dry deposition
121 velocity (V_d) and surface concentration has been commonly applied (Cheng et al., 2012;
122 Luo et al., 2016; Wesely, 1989; Xu et al., 2015; Wen et al., 2020). Notably, there are
123 even fewer studies on the dry deposition of secondary-formation species with neither
124 surface nor satellite observation data available at the regional scale (e.g., nitrate,
125 ammonium, and sulfate). Chemistry transport modeling (CTM), which takes
126 mechanisms of secondary formation of atmospheric species into account, is able to
127 provide the temporal and spatial distribution of ambient concentration of those species,
128 thus can potentially be incorporated into the machine learning framework to improve
129 the deposition estimation and complete the information for individual species. Such
130 application (combination of CTM and machine learning in deposition estimation) has
131 been seldom reported to our knowledge.

132 In response to the above limitations, this study aims to develop a machine
133 learning framework for estimating the historical long-term deposition of multiple N



134 and S species at relatively high horizontal ($0.25^{\circ} \times 0.25^{\circ}$) and temporal resolution
135 (monthly) for China, and to explore the comprehensive impact of the national air
136 pollution controls on the deposition. We select the period 2005-2020, which covers
137 three national FYP periods (11th-13th), NAPPCAP and TYAPFAP. We applied a random
138 forest (RF) method and a generalized additive model (GAM combining different
139 datasets, including ground-level deposition observation, satellite-derived VCDs,
140 meteorological and geographic variables, and CTM simulation, and explore the
141 spatiotemporal variability of dry and wet deposition for the country. The ratios of
142 deposition to emissions (D/E) were then calculated by region and species to illustrate
143 the source-sink relationships of atmospheric pollutants. The outcomes provide
144 scientific basis for further formulating emission control strategies, combining potential
145 ecological risks of deposition.

146 **2. Materials and methods**

147 **2.1 Study domain**

148 We selected Chinese mainland as the research area including 31 provincial-level
149 administrative regions (excluding Hong Kong, Macao and Taiwan). As shown in
150 Figure 1, the 31 provinces are geographically classified into 6 parts, i.e., North Central
151 (NC), North East (NE), North West (NW), South East (SE), South West (SW), and the
152 Tibetan Plateau (TP), representing the diverse social-economical and geo-climatic
153 conditions. The details in climate, population and GDP are provided by region in Table
154 S1 in the Supplement. Basically, NC (with Inner Mongolia excluded) and SE belong to
155 the relatively developed regions in eastern China, NW, SW and NE belong to less
156 developed regions, while TP represents the background region. Bounded by the
157 Qinling Mountain-Huaihe River Line (Figure 1), the climate in the south (SE and SW)
158 is humid with more precipitation than the north (e.g., NC).



159 **2.2 Dry deposition flux estimation**

160 **2.2.1 Random forest (RF) model description**

161 Figure 2 shows the methodology framework of dry and wet deposition simulation.
162 We applied a multisource-fusion RF model to estimate the spatiotemporal pattern of
163 dry deposition for individual N and S species including NO_3^- , HNO_3 , NO_2 , NH_4^+ , NH_3 ,
164 SO_2 , and SO_4^{2-} (H_2SO_4 is not included due to its tiny amount and unavailability of
165 relevant data), at $0.25^\circ \times 0.25^\circ$ horizontal resolution and monthly level for 2005-2020.
166 RF model is a state-of-art statistical method to deal with the complicated nonlinear
167 relationship between response variable and interpretation variables. Briefly, with the
168 ensemble learning, the RF regression predictions are determined as the average of the
169 multiple regression trees based on the bootstrap sampling method (Breiman, 2001).
170 The model performance strongly depends on two crucial parameters, *n_{tree}* (number of
171 the regression trees) and *m_{try}* (number of interpretation variables sampled for splitting
172 at each node), and they were respectively determined at 1000 and 3 to train our model.
173 Not all interpretation variables participate in the process of node splitting (Li et al.,
174 2020b), thus significant correlations of regression trees can be avoided. Besides, the
175 backward variable selection was performed on the RF model to achieve the better
176 performance. Please refer to SI Text Section for the detailed algorithm of the model.

177 We ran the RF modeling program by using the “caret” package in R software
178 (version 4.1.2; Kuhn, 2021). As shown in Figure 2, we firstly selected satellite-derived
179 tropospheric vertical columns densities (VCDs), meteorological factors, geographic
180 covariates and chemical transport mode (CTM) results as interpretation variables, and
181 calculated the dry deposition flux (F_d) at ground observation sites as response variable:

182
$$F_d = C \times V_d \quad (1)$$

183 where C is the estimated (for SO_4^{2-}) or observed concentration (for other species)
184 described in Section 2.2.2, and V_d is the modeled dry deposition rates (V_d) with the



185 Goddard Earth Observation System-Chemistry (GEOS-Chem) 3-D global transport
186 model (<http://geos-chem.org>) described in Section 2.2.4.

187 Secondly, we used the “nearZeroVar” function in “caret” package to eliminate the
188 zero variance variables, to delete highly correlated variables, and to prevent the
189 multicollinearity. Based on the Recursive Feature Elimination (RFE), we then input the
190 final features to the model as summarized in Table S2 in the supplement. The RFE
191 algorithm is a backward selection of features based on the relative importance of
192 interpretation variables (RIV). In order to eliminate the different distributions/ranges
193 caused by the magnitudes of various variables, we mapped them to the same interval
194 through standardization and normalization. Before modeling, the interpretation
195 variables were sorted, and the less important factors were eliminated in turn. Finally,
196 we split the entire model fitting dataset into 10 groups to test the robustness of RF
197 model (10-fold cross validation). In each round of cross validation, the samples in 9
198 groups were used as the training data, and the remaining group was applied for
199 prediction. This process repeated 10 times and every group was tested. The consistency
200 between the calculated F_d (as an observation) and predictions was evaluated using
201 statistical indicators, including coefficient of determination (R^2), root mean squared
202 prediction error (RMSE), mean prediction error (MPE) and relative prediction error
203 (RPE).

204 **2.2.2 Ground-level concentration observations and prediction**

205 The daily ground-level concentrations of NO_2 and SO_2 during 2013-2020 were
206 obtained from the real-time data publishing system of the China National
207 Environmental Monitoring Centre (CNEMC,
208 <http://datacenter.mee.gov.cn/websjzx/queryIndex.vm>), with the abnormal values
209 eliminated. The total number of observation sites reached 1532 in 2020, mainly located
210 eastern China with dense industrial economic and population (e.g., 600 and 408 sites in
211 SE and NC, respectively), as shown in Figure 1. Monthly-level concentrations were



212 then calculated for RF model prediction. The Nationwide Nitrogen Deposition
213 Monitoring Network (NNDMN) established by China Agricultural University contains
214 43 monitoring sites in China (as shown in Figure 1) and measured monthly
215 concentrations gaseous NH_3 , NO_2 , and HNO_3 and particulate NH_4^+ and NO_3^- in air, as
216 well as wet/bulk deposition from 2010 to 2014. The complete datasets of NNDMN
217 were published in previous work (Xu et al., 2019).

218 Due to the lack of large-scale ground observation data, sulfate (SO_4^{2-})
219 concentration must be obtained with an indirect method. Given the significant positive
220 correlation between the two (Luo et al., 2016), we estimated a simple linear
221 relationship between SO_2 and sulfate concentration with CTM and calculated the
222 sulfate concentrations ($G_{\text{SO}_4^{2-}}$):

$$223 \quad G_{\text{SO}_4^{2-}} = G_{\text{SO}_2} \times f(G_{\text{CTM-SO}_4^{2-}}, G_{\text{CTM-SO}_2}) \quad (2)$$

224 where G_{SO_2} is the monthly ground-level concentration at CNEMC; $G_{\text{CTM-SO}_4^{2-}}$,
225 $G_{\text{CTM-SO}_2}$ are the sulfate and SO_2 concentrations simulated by CTM, respectively, and
226 f is the ratio of simulated sulfate to SO_2 (see Section 2.2.4 for CTM description).

227 2.2.3 Satellite-derived VCDs

228 The tropospheric VCDs of NO_2 from 2005 to 2020 were taken from Peking
229 University OMI NO_2 tropospheric product version2 (POMINO v2; Liu et al., 2019),
230 based on the observation of Ozone Monitoring Instrument (OMI). The VCDs with
231 cloud coverage over 25% were eliminated as high cloudiness would distort satellite
232 detection and increase inversion error. The daily SO_2 VCDs were obtained from
233 Level-3e OMSO2 Data Products from 2005 to 2020
234 (https://disc.gsfc.nasa.gov/datasets/OMSO2e_003/summary). All the OMI SO_2 data
235 were generated by an algorithm based on principal component analysis (PCA), which
236 was considerably sensitive to anthropogenic emissions (Krotkov et al., 2016). The total



237 VCDs of NH_3 were derived from the Infrared Atmospheric Sounding Interferometer
238 (IASI), board on MetOp-A platform. The standard daily IASI/Metop-A ULB-LATMOS
239 total column Level-2 product v2.2.0 is available from 2008 to 2020
240 (https://iasi.aeris-data.fr/nh3_iasi_a_arch/). The daily total column was excluded when
241 the cloud coverage was $>25\%$, the relative error was $>100\%$, or the absolute error
242 was $>5 \times 10^{15}$ molecules cm^{-2} (Whitburn et al., 2016). The NH_3 VCDs from 2005 to
243 2008 were estimated based on the linear correlations between NH_3 emission and VCDs
244 during 2008-2020.

245 We used the Kriging interpolation method to fill the missing values, and obtained
246 the spatial pattern of VCDs at the horizontal resolution of $0.25^\circ \times 0.25^\circ$. Monthly-level
247 VCDs were calculated based on the daily products from 2005 to 2020.

248 **2.2.4 CTM model description**

249 We used GEOS-Chem v12.1.1 to simulate the V_d and the ground-level
250 concentrations of individual species. A nested version was applied with the native
251 horizontal resolution of $0.5^\circ \times 0.625^\circ$ over East Asia ($70\text{--}150^\circ\text{E}$, $11^\circ\text{S}\text{--}55^\circ\text{N}$) and $4^\circ \times 5^\circ$
252 for rest of the world, and the simulated V_d and concentrations within China were
253 spatially interpolated at the resolution of $0.25^\circ \times 0.25^\circ$. As described in Section 2.2.1,
254 the V_d for 2013-2018 was calculated based on a standard big-leaf resistance-in-series
255 parameterization (Wesely, 1989), and applied in estimation of the response variable dry
256 deposition flux. The simulated concentrations of individual species since 2005 were
257 used as the interpretation variable in RF.

258 The model was driven by the MERRA-2 assimilated meteorological data provided
259 by the Global Modeling and Assimilation Office (GMAO) at the National Aeronautics
260 and Space Administration (NASA). Meteorology fields such as vertical pressure
261 velocity, temperature, surface pressure, relative and specific humidity had a temporal
262 resolution of 3 h, and surface variables (such as sea level pressure, tropopause pressure)



263 and mixing depths were at 1 h resolution. The model had 47 vertical layers from
264 surface to 0.01 hPa, and the lowest layer is centered at 58 m above sea level.

265 Emissions in GEOS-Chem were processed through Harvard–NASA Emission
266 Component (HEMCO; Keller et al., 2014). We used the Community Emissions Data
267 System for global anthropogenic emissions, overwritten by the regional emissions
268 inventories in the USA, Europe, Canada and Asia, involving the National Emissions
269 Inventory from EPA (NEI;
270 <https://www.epa.gov/air-emissions-inventories/air-pollutant-emissionstrends-data>),
271 European Monitoring and Evaluation Programme emissions (EMEP; European
272 Monitoring and Evaluation Programme; www.emep.int/index.html) and the MIX
273 inventory that included MEIC over China. Natural NO_x sources from soil and
274 lightning were also included (Lu et al., 2021).

275 **2.2.5 Other data**

276 The meteorological parameters for 2005-2020, including precipitation, boundary
277 layer height, temperature at two meters, wind speed, wind direction, surface pressure,
278 total column, total column ozone, were downloaded from the European Centre for
279 Medium-Range Weather Forecasts (ECMWF,
280 <https://apps.ecmwf.int/datasets/data/interim-full-daily/levtype=sfc/>) at the resolution of
281 0.25°× 0.25°.

282 Land-Use and Land-Cover Change (LUCC), Digital Elevation Model (DEM),
283 population density data (POP) and Gross Domestic Product (GDP) were obtained from
284 Chinese Resource and Environment Data Cloud Platform (<http://www.resdc.cn/>).
285 Except for the DEM, other data were compiled at a five-year interval (2005, 2010 and
286 2015 for this study). LUCC was generated by manual visual interpretation of Landsat
287 TM/ETM remote sensing image. We calculated the area fractions of different land use
288 in the buffer zone (60 km in diameter around each site). The elevation spatial



289 distribution data (DEM) were extracted from the Shuttle Radar Topography Mission at
290 the 1-km resolution, assuming no variability during the study period. For GDP and
291 POP, datasets with 1-km resolution were developed through spatial interpolation,
292 taking their spatial interactions with land use type and night light brightness into
293 account (Xu, 2017). Linear interpolation was applied to complete the information for
294 all the years within the research period, and all the above-mentioned interpretation
295 variables were resampled to a uniform horizontal resolution of $0.25^{\circ} \times 0.25^{\circ}$.

296 **2.3 Wet deposition flux estimation**

297 As shown in Figure 2, we applied a nonlinear Generalized Additive Model (GAM)
298 developed in our previous work (Zhao et al., 2022) to estimate the monthly wet
299 deposition of SO_4^{2-} , NO_3^- and NH_4^+ in China at a horizontal resolution of $0.25^{\circ} \times 0.25^{\circ}$:

$$300 \quad g(\mu_m) = \sum_{i=1}^n f_i(x_{i,m}) + \sum_{p,q} f_{pq}(x_{p,m}, x_{q,m}) + X_m\theta + \varepsilon_m \quad (3)$$

301 where g is the “link” function, which specifies the relationship between the response
302 variable μ and the linear formulation on the right side of equation; $f_i(x_i)$ is the nonlinear
303 smooth function that explores the single effect of individual interpretation variable x_i ;
304 m indicates the month; n represents the total number of interpretation variables for
305 which single effect was considered in the model; $f_{pq}(x_p, x_q)$ is nonlinear smooth
306 function that explores the interaction effect of interpretation variable x_p and x_q ; $X\theta$
307 represents an ordinary linear model component for interpretation variables (elements of
308 the vector X) not subject to nonlinear transformations; and ε represents the residuals of
309 models. The smooth functions $f_i(x_i)$ and $f_{pq}(x_p, x_q)$ are fitted by thin-plate regression
310 splines and tensor product smoothing, respectively. With an assumption of normal
311 distribution, Gaussian distribution and the log link function are applied for the model
312 residuals.

313 For SO_4^{2-} , the observation data of monthly wet deposition were collected from the



314 East Asia Acid Deposition Monitoring Network (EANET) as response variables. For
315 NO_3^- and NH_4^+ , the observed monthly wet or bulk deposition at NNDMN served as the
316 response variables. For all the three species, the interpretation variables contained the
317 precipitation, satellite-derived VCDs, $\text{PM}_{2.5}$ concentrations, total column liquid water,
318 temperature, boundary layer height, forest-cover and urban-cover. The data sources and
319 model performance evaluation was described in Zhao et al. (2022). Although bulk
320 deposition includes a small amount of dry deposition, the deposition in precipitation
321 obtained through GAM was uniformly defined as wet deposition in this work.

322 **3. Results and discussions**

323 **3.1 RF model prediction performance**

324 The RF model performances for dry deposition estimation evaluated with 10-fold
325 cross validation are shown in Figures S1 and S2 in the supplement based on CNEMC
326 and NNDMN, respectively. The multi-year average R^2 of N and S species over China
327 were all above 0.7 and the RMSE of all models were less than $1 \text{ kg N/S ha}^{-1} \text{ yr}^{-1}$
328 except for NO_2 ($1.09 \text{ kg N ha}^{-1} \text{ yr}^{-1}$) and SO_2 ($6.46 \text{ kg S ha}^{-1} \text{ yr}^{-1}$), indicating the
329 satisfying consistency between observation and prediction. However, the model tended
330 to underestimate the high deposition and overestimate the low one possibly because the
331 model algorithm based on the average of all regression trees resulted in relatively weak
332 estimation of the extreme values. The modeling prediction performance of OXN (NO_3^- ,
333 HNO_3 and NO_2) was clearly better than that of RDN (NH_4^+ and NH_3) and sulfur (SO_2
334 and SO_4^{2-}). For example, the R^2 of NO_2 , NO_3^- and HNO_3 were 0.87, 0.73 and 0.78,
335 while those of NH_3 and NH_4^+ were only 0.71 and 0.65. POMINO, which reduced the
336 bias of the default product by the OMI Nitrogen Dioxide Algorithm Team (Krotkov et
337 al., 2019; Liu et al., 2019), was demonstrated to be satisfyingly applicable in OXN
338 deposition prediction for China. In addition, the prediction performances of CNEMC
339 were better than those of NNDMN (except for SO_2), attributed partly to much more



340 monitoring stations for the former. As indicated in our previous work, improved model
341 performance could be expected along with the increased abundance of observation data
342 (Zhou et al., 2021).

343 To evaluate the long-term average deposition from RF modeling, we collected 34
344 studies that quantified the deposition of different species and forms (dry or wet) for
345 China using observational, geostatistical or modal methods (Table S3 in the
346 supplement). As shown in Figure 3, gaseous NH_3 and SO_2 were identified as the
347 species with largest dry deposition, while sulfate as the species with the largest wet
348 deposition. The multi-year averages (2005-2020) of dry deposition for different species
349 estimated in this study were within the range between 25th Quantile (Q1) and 75th
350 Quantile (Q3) of selected studies except for NH_3 (Figure 3a), but that of sulfate wet
351 deposition closing to Q1 was basically lower compared to existing studies (Figure 3b).
352 Most of the existing studies reported sulfate wet deposition in China for 2001-2005
353 when the national control of SO_2 emissions and acid rain was still in its initial stage,
354 while limited data was available for more recent years when sharp declines were found
355 for SO_2 emissions. Therefore, the average of existing studies might potentially
356 overestimate the actual average level of S deposition across the country. Overall, the
357 total deposition of N and S from RF modeling was satisfyingly closed to the median
358 level of the existing studies (Figure 3c), indicating the robustness of deposition
359 estimation.

360 We calculated the shares of different forms and species to the average of national
361 total deposition in 2005-2020 (Figure 4). The dry deposition of N followed an order of
362 $\text{NH}_3 > \text{HNO}_3 > \text{NO}_2 > \text{NH}_4^+ > \text{NO}_3^-$, while the wet NH_4^+ deposition was larger than NO_3^- .
363 As a whole, RDN (58%) was found to contribute more than OXN (42%) to the total N
364 deposition. For S species, the dry deposition of SO_2 was over ten times of SO_4^{2-} , while
365 the latter was only species of wet deposition. Dry deposition was estimated to be
366 higher than wet for both N and S, with its fraction reaching 70% and 65% within the



367 research period, respectively. The more specific interannual variability and spatial
368 distribution for different forms will be described in Sections 3.2 and 3.3.

369 **3.2 Temporal variability in deposition of Nr species and sulfur**

370 Based on the newly developed RF method, the average dry deposition of OXN,
371 RDN, total N and S in China were estimated at 10.4, 14.4, 24.9 and 16.7 kg N/S ha⁻¹
372 yr⁻¹ from 2005 to 2020, respectively. The total deposition reached 15.2, 20.2, 35.4 and
373 25.9 kg N/S ha⁻¹ yr⁻¹, respectively, when the average wet deposition estimated with
374 GAM (Zhao et al., 2022) was included. Figure 5a-d illustrates the long-term
375 interannual variability of dry and wet deposition for OXN, RDN, total N and S,
376 respectively. Different temporal trends are found for N and S, due partly to the diverse
377 of their precursor emissions. As indicated by MEIC, China's NO_x emission control was
378 limited before 2012, allowing annual national emissions to grow 49% from 2005 to
379 2012 (Figure 5f). Starting in 2013, NAPPAP drove fast growing penetration of
380 selective catalyst reduction (SCR) systems in the power and cement production sectors,
381 resulting in a 28.6% reduction in the annual total emissions of NO_x from 2013 to 2020
382 (Karplus et al., 2018; Li et al., 2018). Similar temporal variability was found for OXN
383 deposition: it was increasing slightly from 14.7 in 2005 to 15.7 kg N ha⁻¹ yr⁻¹ in 2012,
384 and then declining to 14.5 kg N ha⁻¹ yr⁻¹ in 2020 (Figure 5a). The interannual variation
385 in NH₃ emissions has been much smaller than NO_x, with a slight reduction by 9% from
386 2005 to 2020 (Figure 5f), attributed to the changes in Chinese agricultural practices,
387 e.g., improved waste management in livestock farming and replacement of highly
388 volatile ammonium bicarbonate with urea in fertilizer types (Liu et al., 2017b; Zheng et
389 al., 2018b). However, the big emission abatement of acidic gases like SO₂ after 2013
390 was recognized to reduce the sink of NH₃ in the atmosphere and to increase of
391 gas-phase NH₃ concentrations (Liu et al., 2018), resulting in more dry NH₃ deposition
392 (Figure 5b). After 2015, China's RDN deposition became relatively stable, which could
393 be partly explained by the implementation of Zero Increase Action Plan for N fertilizer



394 after 2015 (Liu et al., 2022). As a combined effect of changing emissions and
395 atmospheric conditions, the RDN deposition was estimated to grow from 19.5 in 2005
396 to 20.6 kg N ha⁻¹ yr⁻¹ in 2020. China has widely applied flue gas sulfurization (FGD)
397 in the power sector since 2005, and has expanded its application to other industries
398 (such as sintering furnaces and non-electric coal-fired boilers) since 2013, as a part of
399 NAPPAP (Zheng et al., 2018a). As a result, the annual national SO₂ emissions were
400 estimated to decline by 76% from 2005 to 2020 (Figure 5f), and the dry deposition of S
401 by 31% (Figure 5d). The wet deposition was less responsive to emissions than dry
402 deposition, and the growth in precipitation was likely offsetting part of the benefit of
403 emission control on wet deposition (Zhao et al., 2022). The total S deposition was
404 calculated to decline 26%, from 28.8 in 2005 to 21.3 kg S ha⁻¹ yr⁻¹ in 2020.

405 Shown in Figure 5a-d as well is the long-term interannual variability of the dry to
406 wet deposition ratio ($R_{\text{dry/wet}}$) during 2005-2020. The $R_{\text{dry/wet}}$ of N species kept
407 relatively stable for earlier years and then gradually increased since 2015, with the
408 multi-year average ratios estimated at 2.2, 2.5 and 2.4 for OXN, RDN and total N,
409 respectively. The $R_{\text{dry/wet}}$ of sulfur declined before 2015 and then slightly increased
410 afterwards, with the average ratio estimated at 1.8 for 2005-2020. The growth of
411 $R_{\text{dry/wet}}$ of RDN could be partly attributed to the improved control of acid precursor
412 emissions for recent years. Since 2013, as mentioned above, implementation of
413 NAPPAP and abatement of SO₂ emissions has reduced the sink of NH₃ in the
414 atmosphere, elevating the free ammonia in the air and thereby $R_{\text{dry/wet}}$ of RDN.
415 Significant negative correlation coefficient between precipitation and $R_{\text{dry/wet}}$ was found
416 for both OXN (-0.63) and S (-0.64), indicating the influence of precipitation. Notably,
417 precipitation increased at a rate of 6.3 mm yr⁻¹ in China during 2005-2015 (Figure S3
418 in the supplement), motivating the formation of wet deposition of SO₂ that is easily
419 soluble in water. The declining precipitation after 2015 resulted in the reduced wet
420 deposition and thereby enhanced $R_{\text{dry/wet}}$ for OXN and S. In addition, the increased



421 temperature after 2012 (Figure S3) could strengthen the atmospheric diffusion and the
422 opening of stomata of plant leave, which in turn resulted in more pollutants being
423 removed via dry deposition (Zhang et al., 2004).

424 Figure 5e shows the long-term interannual variability of the ratio of RDN to OXN
425 deposition ($R_{\text{RDN/OXN}}$) for different forms during 2005-2020. $R_{\text{RDN/OXN}}$ indicates the
426 relative contributions of industrial and agricultural activities to N deposition, as the
427 major anthropogenic sources of RDN are animal excrement and fertilizer use in
428 agriculture while those of OXN are fossil fuel combustion in power, industrial and
429 transportation sectors (Pan et al., 2012; Zhan et al., 2015; Zhu et al., 2015). $R_{\text{RDN/OXN}}$ is
430 estimated to be larger than 1 for the whole research period, with a continuous decline
431 from 2005 to 2011 and more prominent rebound afterwards, and it reached 1.5 for total
432 N in 2020. The ratio for dry deposition was larger than the wet one. The declining
433 $R_{\text{RDN/OXN}}$ resulted mainly from the growth of NO_x emissions and thereby OXN
434 deposition, driven by the fast development of industrial economy and increasing fossil
435 fuel combustion. The growing $R_{\text{RDN/OXN}}$ since 2012 was expected to be largely driven
436 by the continuous efforts of NO_x emission controls, and highlighted the benefit of
437 those efforts on limiting OXN pollution. Regulation on NH_3 emission controls, mainly
438 in agricultural activities, became increasingly important for further alleviating the N
439 pollution.

440 As summarized in Table S4 in the supplement, the annual average deposition of N
441 and S in China was much larger than that for USA estimated by Clean Air Status and
442 Trends Network (CASTNET, <https://www.epa.gov/castnet>) and National Atmospheric
443 Deposition Programme (NADP, <https://nadp.slh.wisc.edu/networks/national-trends-network/>) and Europe by European
444 Monitoring and Evaluation Programme (EMEP, <https://projects.nilu.no/ccc/index.html>).
445 According to Vet et al. (2014), the ensemble-mean results of 21 global CTMs indicated
446 that eastern China was the region with the highest nitrogen deposition in the world,
447



448 with a value of $38.6 \text{ kg N ha}^{-1} \text{ yr}^{-1}$. Compared with USA and Europe, China has not
449 only experienced high deposition of N and S but also featured the greatest increase
450 over the past decade (Du and Liu, 2014; Fu et al., 2022; Jia et al., 2016). Figure 6
451 illustrates the interannual variations of emissions, deposition and $R_{\text{RDN/OXN}}$ for China as
452 well as the more developed USA and Europe (28 countries). The emission data for the
453 three continents were respectively taken from MEIC, the U.S. Environmental
454 Protection Agency (EPA, <https://www.epa.gov/air-emissions-inventories/air-pollutant-emissionstrends-data>), and
455 European Environment Agency (EEA, <https://www.eea.europa.eu/themes/air>). As
456 shown in Figure 6a and 6c, the interannual trends in estimated deposition were
457 basically consistent with those in emissions, with observed reduction for both OXN
458 and S deposition over the USA and Europe. With the slowdown in economic growth
459 and the implementation of air pollution control actions for decades (e.g., Clean Air Act
460 (CAA) in the USA and Convention on Long-range Transboundary Air Pollution
461 (CLRTAP) in Europe), the emissions of NO_x and SO_2 have been reduced by more than
462 60% and 90% in between 1980 and 2020, respectively (Fowler et al., 2013). However,
463 as a result of the rapidly growing demand for economic development and energy, the
464 fossil fuel consumption and fertilizer utilization increased by 3.2 and 2.0 times
465 during 1980-2010 for China, which ultimately led to an increase in the OXN and RDN
466 deposition from 2005 to 2010 (An et al., 2019; Li, 2020; Liu et al., 2020). Following
467 developed countries, gradually tightened measures of reducing the acidifying air
468 pollutants have been launched since 2005, and the deposition began to decline
469 afterwards.

471 We selected the periods with fast declines in deposition of OXN and S for the
472 three continents and compared them in Table 1. The relative changes in deposition
473 were smaller than those of emissions for all the continents, and greater declines were
474 found for S for both emissions and deposition than OXN. Compared with Europe and



475 the USA, China had the smallest benefit of precursor emission abatement on deposition.
476 For example, the SO₂ emissions in the USA, Europe and China had been cut by 78.4%
477 (2003-2016), 57.6% (2000-2013) and 75.5% (2007-2020) respectively, while S
478 deposition had declined by 72.5%, 49.9% and 27.0%. This may be caused by a lagging
479 response of deposition to emission abatement, which is more prominent in China.
480 Europe and the USA started emission controls earlier than the selected periods, resulted
481 in a smaller gap between the changes in emissions and deposition afterwards. The
482 comparison implies that the effect of short-term emission reduction in China would not
483 immediately be fully reflected in the deposition, but continuous efforts on emission
484 abatement should be made to achieve substantial reduction in deposition and to further
485 mitigate ecological risks.

486 Figure 6d presents the interannual changes of $R_{\text{RDN/OXN}}$ for China, USA, and
487 Europe (28 countries). The $R_{\text{RDN/OXN}}$ in China was higher than those in the other two,
488 with an average of 1.3 in 2005-2020 (0.9 and 1.0 for the USA and Europe during the
489 same period). As a developing country, China is an important food producing country
490 in the world, with a long history of agricultural production and planting. Large
491 agricultural production and relatively weak policy management made China the largest
492 NH₃ emissions in the world, leading to a high proportion of RDN deposition to the
493 total N deposition (Kang et al., 2016; Liu et al., 2022). In contrast, in developed USA
494 and Europe with high level of agricultural mechanization and abundant industry and
495 transportation, the relatively high NO_x emissions compared to NH₃ resulted in smaller
496 $R_{\text{RDN/OXN}}$ than China.

497 Similar temporal changes in $R_{\text{RDN/OXN}}$ can be found for USA and China, i.e.,
498 decline in earlier years and growth afterwards. For USA, the turning point of $R_{\text{RDN/OXN}}$
499 occurred in 1999, 13 years earlier than that of China in 2012. The turning points were
500 closely associated with the introduction and implementation of NO_x emission controls
501 for the two countries (CAA Amendments since 1990 for the USA and NAPPcap since



502 2013 for China). While RDN in China has been the major species since 2005, the OXN
503 in the USA was larger than RDN for over 20 years. The $R_{\text{RDN/OXN}}$ kept growing since
504 2000 and exceeded 1 in 2014, indicating a transition of major N species in the
505 deposition. Different from China and the USA, $R_{\text{RDN/OXN}}$ in Europe kept declining
506 since 2000, and being smaller than 1 after 2013. In many European countries with
507 abundant agricultural activities, the chemical fertilizer and livestock breeding release a
508 large amount of NH_3 . Europe attached great importance to the source control of
509 agricultural pollution, adopted the economic guidance method for agricultural
510 environmental subsidies, and member states actively assumed the responsibility for
511 governance for decades (i.e., Common Agriculture Policy, CAP; Zhang et al., 2020).
512 Therefore, the control of NH_3 in Europe was ahead of China, resulting in continuous
513 reduction in NH_3 emissions and thereby $R_{\text{RDN/OXN}}$.

514 3.3 Spatial variability in deposition of Nr species and sulfur

515 Figure 7 shows the spatial distributions of N and S deposition fluxes during
516 2005-2020. In general, relatively large deposition was found in eastern China with
517 more population and developed industrial economy (e.g., SE and part of NC in Figure
518 1). Hotspots of dry deposition were commonly located in the north while wet in the
519 south. As a joint effect of concentrations and V_d , high level of OXN dry deposition was
520 estimated in areas with high vegetation cover, such as Yunnan and Fujian province. For
521 S dry deposition, coal-fired boilers for power and heating were intensively distributed
522 in the north, leading to abundant SO_2 emissions and thereby dry deposition.
523 Furthermore, the relatively stable weather conditions with less convection in the north
524 was unfavorable to the dispersion and dilution of pollutants. The emissions were thus
525 liable to be deposited locally. For RDN, the agricultural production, animal husbandry
526 and biomass burning in NC and the northern part of SE led to relatively NH_3 emissions
527 and thereby high dry deposition. The more acidic and humid soils in the south made
528 NH_3 more difficult to release, resulting in lower dry deposition compared to the north.



529 Large wet deposition was mainly found in the south of China associated with the
530 uneven distribution of precipitation. In summer, the air masses in the western Pacific
531 Ocean and the South China Sea were affected by the southeast and southwest monsoon,
532 significantly increasing the rainfall in southeast China. For the total deposition (wet
533 plus dry), the high deposition of OXN and S were located in SE, while RDN and total
534 N were mainly concentrated in NC and the north of SE.

535 As shown in Table S5 in the Supplement, the $R_{\text{dry/wet}}$ of N and S in the eastern
536 China (SE+NC with Inner Mongolia excluded) was smaller than that in western China
537 (NW+TP), attributed mainly to the large precipitation in the former. Given the dry
538 climate and less anthropogenic activities, the pollution was mainly transported by
539 atmospheric turbulence and removed from the atmosphere by dry deposition in western
540 country. The $R_{\text{dry/wet}}$ of TP was the highest out of the six regions, with 2.6 and 3.7 for
541 total N and S, respectively. The $R_{\text{dry/wet}}$ in NE, NW and NC was generally higher than
542 that in the south (SE and SW), resulting also from the abundant precipitation in the
543 south. Higher $R_{\text{RDN/OXN}}$ was found in the west (e.g., NW and TP) and lower in the east
544 (Table S5), as more developed industry in the east resulted in relatively large NO_x
545 emissions and thereby OXN deposition, while farming and animal husbandry
546 dominated the economy in the west, leading to substantial NH₃ emissions.

547 Figure 8 and Table 2 compare the relative changes of total deposition (wet plus
548 dry) of different species for eastern, western and whole country. The interannual
549 changes of deposition for all species were smaller than that of emissions (Table 2),
550 reconfirming lagging response of deposition to changing emissions as mentioned in
551 Section 3.2. During the period when emissions declined rapidly, the change of
552 deposition has not yet occurred. The relative changes for N and S deposition in eastern
553 China were generally larger than the whole country, indicating the effectiveness of
554 extremely stringent emission controls on those regions with abundant emissions from
555 industrial and traffic sources. The OXN deposition for all the concerned regions shows



556 an invert “V” pattern over time, consistent with the progress of NO_x emissions control
557 (Figure 8a). The relative annual changes in eastern China (9% in 2005-2012 and -12%
558 in 2012-2020) were generally greater than in western (4% in 2005-2012 and -5% in
559 2012-2020). More specifically, the turning point for western China was later than the
560 East, likely resulting from later implementation of emission control policies. Most
561 measures were first implemented in the highly developed key regions in east and then
562 applied more widely afterwards. As shown in the Figure 8b and Table 2, RDN
563 deposition was relatively stable before 2012, and the temporal changes in eastern and
564 western China were generally consistent with each other. The lack of comparable
565 control policies for NH₃ and strict policy of acid precursors likely explained the
566 increasing trend in RDN afterwards, with 9% in eastern and 10% in western China
567 between 2012 and 2020. The biggest reduction was achieved for S deposition, and the
568 decline in eastern China was faster than that in the western (Figure 8c). Attributable to
569 the earlier and broader use of FGD at coal combustion sources, greater abatement of
570 SO₂ emissions was achieved than NO_x or NH₃ over the past decade, leading to the
571 faster reduction in S deposition than in OXN or RDN (Table 2). In addition, the
572 reduction during 2012-2020 (28%, 18% and 21% for the eastern, western and the
573 whole country, respectively) was clearly larger than that during 2005-2012 (3%, 9%
574 and 7%, respectively), indicating the greatly improved SO₂ controls compared to
575 earlier years.

576 The ratio of deposition to emissions (D/E) is used to analyze the interactions
577 between the pollutant sources and sinks. Figure 9a shows the annual mean D/E ratios
578 during 2005-2020 by species and region. The D/E in eastern China (e.g., NC and SE)
579 was generally smaller than in western China (NW, SW and TP). The low D/E identified
580 those regions as the major sources of air pollutants due mainly to their intensive
581 emissions, likely influencing air pollution levels in surrounding regions. With less
582 industry, energy consumption and population, by contrast, western China received



583 relatively high deposition compared to local emissions, resulting in large D/E. The very
584 high ratio of D/E indicated that TP was strongly influenced by regional pollution
585 transport. The D/Es of RDN in the six regions were higher than that of OXN and sulfur
586 (except for TP). Due to its relatively short life time, most of NH₃ deposits near the
587 source area, while stronger transport and chemical reaction may occur for NO_x and
588 SO₂ given their longer life time. Significantly positive correlations were found between
589 regional deposition and emissions for all the concern species, with R² estimated at 0.81,
590 0.92, and 0.78 for OXN (Figure 9b), RDN (Figure 9c), and S (Figure 9d), respectively.
591 The result implies that the N and S deposition to the six regions were strongly
592 dependent on the spatial pattern of anthropogenic emissions.

593 The annual emissions, deposition and D/E by land use type were displayed in
594 Table S6 in the supplement. High deposition was commonly found in areas with high
595 energy consumption and large emissions, such as urban and construction sites.
596 Associated with different human activities, moreover, the D/E for sulfur and OXN
597 were smaller in urban regions than those in rural ones, whereas that for RDN was
598 slightly larger in urban areas. Transportation and industries resulted in larger NO_x and
599 SO₂ emissions in urban locales and agricultural activities enhanced NH₃ in rural ones.

600 Figure 10 shows the spatial distribution of multi-year average deposition by
601 season, which was influenced jointly by varying meteorology and emissions. Basically,
602 larger deposition was found in summer than that in winter, and the seasonal difference
603 was particular bigger for N. The deposition in summer was estimated to be 1.9 and 1.6
604 times in winter for OXN and RDN, respectively, while the ratio was much smaller at
605 1.1 for S. The hotspot of deposition was commonly found in NC and northern SE in
606 summer, while it moved to central SE in winter attributed partly to the prevailing
607 northwesterly wind.



608 **3.4 Uncertainties**

609 Uncertainties existed in current analysis. First, the estimated dry deposition or V_d
610 could not be fully examined with sufficient data from direct observation, attributed
611 mainly to the lack of field measurements. Micrometeorological methods can be used
612 for direct observation of dry deposition, including eddy correlation method, gradient
613 method and relaxation vortex accumulation method. Due to the need for extremely fast
614 response instruments and uniform underlying surfaces, those methods have not yet
615 been widely applied in a long-term and extensive manner. Second, error may come
616 from ground-level monitoring data. We collected available data from different
617 monitoring networks, and ignored the difference in observed deposition from diverse
618 methods of sample collection and measurement. Moreover, current RF model relied on
619 the data from observation sites, most of which are located in the eastern China with
620 dense population and developed economy. The model accuracy for remote areas (such
621 as NW and TP) should be further evaluated when more observation data get available
622 for those areas. Third, there was additional uncertainty in the estimation of sulfate dry
623 deposition, as there were limited observed ambient concentrations of sulfate available
624 for estimation of dry deposition, and CTM had to be applied. Furthermore, bulk
625 deposition obtained from the open precipitation gauge contains part of dry deposition
626 and therefore likely overestimate actual wet deposition. The bias varied by region and
627 was hard to be quantified at the national level. For example, research indicated that the
628 dry deposition accounted for around 20% of the bulk deposition based on observation
629 at three rural stations on the North China Plain, and this contribution could reach 39%
630 in urban areas (Zhang et al., 2015; Zhang et al., 2008). Along with continuous
631 development of monitoring networks and increasing availability of deposition data for
632 diverse species, those uncertainties can be further reduced and more accurate
633 deposition estimation can be expected.



634 **4. Conclusions**

635 We developed a full N and S deposition dataset for mainland China at the
636 horizontal resolution of 0.25° for 2005-2020, combining the ground-level observations,
637 satellite-derived VCDs, meteorological and geographic information, and CTM. Based
638 on the newly developed RF method, the annual average dry deposition of OXN, RDN
639 and S in China was estimated at 10.4, 14.4 and 16.7 kg N/S $\text{ha}^{-1} \text{yr}^{-1}$, while the total
640 deposition reached 15.2, 20.2 and 25.9 kg N/S $\text{ha}^{-1} \text{yr}^{-1}$, respectively, with the wet
641 deposition estimated with a GAM model included. The $R_{\text{dry/wet}}$ of N kept relatively
642 stable at the beginning and then gradually increased, especially for RDN, while that of
643 S declined for over 10 years and then slightly increased. Within the whole study period,
644 $R_{\text{RDN/OXN}}$ was estimated to be greater than 1 and clearly larger than that of the USA and
645 Europe, with a continuous decline from 2005 to 2011 and a growth afterwards. The
646 frequent agricultural activities and relatively weak management of manure have
647 resulted in abundant NH_3 emissions and thereby a high proportion of RDN deposition.
648 Improved NO_x emission control was the main reason for the elevated $R_{\text{RDN/OXN}}$ for
649 recent years. Compared with Europe and the USA, China had the smallest benefit of
650 precursor emission reduction on deposition. The prominent lagging response of
651 deposition to emission abatement requires a continuous long-term emission control
652 efforts to substantially reduce atmospheric deposition. As a joint effect of emissions
653 and individual meteorological factors, a downward gradient from east to west was
654 found for dry deposition of OXN while from north to south for S. The wet deposition
655 frequently occurred in the south of China, associated with the spatial distribution of
656 rainfall. The deposition of OXN and S declined faster in eastern China than that in the
657 west after 2012, indicating the effectiveness of extremely strict emission control in
658 developed areas with abundant emissions from industry and transportation. The D/E in
659 eastern China was generally smaller than that in west, as the former was the major
660 sources of air pollutants and the latter received relatively high deposition through
661 regional transport. At the national scale, the deposition strongly depended on the



662 spatial pattern of anthropogenic emissions within the regions. The current study
663 broadens the scientific understanding of China's long-term changes in deposition of
664 typical atmospheric species, as well as the influences of human activities and emission
665 controls. More observation and modeling work is recommended for in-depth analyses
666 on the complicated and changing relationship between emissions and deposition for
667 specific species, as well as the consequent varying effects on ecosystem.

668 **Data availability**

669 The multiyear deposition data by species at the horizontal resolution of 0.25° will be
670 available at <http://www.airqualitynju.com/En/Data/List/Datadownload> once the paper
671 is published.

672 **Author contributions**

673 KZhou developed the methodology, conducted the research, performed the analyses
674 and wrote the draft. YZhao developed the strategy, designed the research and revised
675 the manuscript. LZhang and MMA provided the support of air quality modeling. WXu
676 and XLiu provided the support of NNDMN data.

677 **Competing interests**

678 The authors declare that they have no conflict of interest.

679 **Acknowledgements**

680 This work was sponsored by the Natural Science Foundation of China (42177080) and
681 the Key Research and Development Programme of Jiangsu Province (BE2022838). We
682 acknowledge Qiang Zhang from Tsinghua University for the emission data (MEIC),
683 and Jintai Lin from Peking University for the satellite data (POMINO v2).

684 **References**

685 An, Z., Huang, R. J., Zhang, R., Tie, X., Li, G., Cao, J., Zhou, W., Shi, Z., Han, Y., Gu,
686 Z., and Ji, Y.: Severe haze in northern China: A synergy of anthropogenic



- 687 emissions and atmospheric processes, Proc. Natl. Acad. Sci., 116, 8657-8666,
688 <https://doi.org/10.1073/pnas.1900125116>, 2019.
- 689 Baker, L. A., Herlihy, A. T., Kaufmann, P. R., and Eilers, J. M.: Acidic Lakes and
690 Streams in the United States: The Role of Acidic Deposition, Science, 252,
691 1151-1154, <https://doi.org/10.1126/science.252.5009.1151>, 1991.
- 692 Beachley, G., Puchalski, M., Rogers, C., and Lear, G.: A summary of long-term trends
693 in sulfur and nitrogen deposition in the United States: 1990-2013, JSM environ.
694 sci. ecol., 4, 1030-1034, 2016.
- 695 Breiman, L.: Random forests, Mach. Learn., 45, 5-32,
696 <https://doi.org/10.1023/a:1010933404324>, 2001.
- 697 Burns, D. A., Aherne, J., Gay, D. A., and Lehmann, C. M. B.: Acid rain and its
698 environmental effects: Recent scientific advances, Atmos. Environ., 146, 1-4,
699 <https://doi.org/10.1016/j.atmosenv.2016.10.019>, 2016.
- 700 Cheng, M., Jiang, H., Guo, Z., Zhang, X., and Lu, X.: Estimating NO₂ dry deposition
701 using satellite data in eastern China, Int. J. Remote Sens., 34, 2548-2565,
702 <https://doi.org/10.1080/01431161.2012.747019>, 2012.
- 703 Cheng, I. and Zhang, L.: Long-term air concentrations, wet deposition, and scavenging
704 ratios of inorganic ions, HNO₃ and SO₂ and assessment of aerosol and
705 precipitation acidity at Canadian rural locations, Atmos. Chem. Phys., 17,
706 4711-4730, <https://doi.org/10.5194/acp-17-4711-2017>, 2017.
- 707 Cheng, I., Zhang, L., He, Z., Cathcart, H., Houle, D., Cole, A., Feng, J., O'Brien, J.,
708 Macdonald, A. M., Aherne, J., and Brook, J.: Long-term declines in atmospheric
709 nitrogen and sulfur deposition reduce critical loads exceedances at multiple
710 Canadian rural sites, 2000–2018, Atmos. Chem. Phys., 22, 14631-14656,
711 <https://doi.org/10.5194/acp-22-14631-2022>, 2022.
- 712 Du, E. and Liu, X.: High rates of wet nitrogen deposition in China: A synthesis, in:
713 nitrogen deposition, critical loads and biodiversity, edited by: Sutton, M. A.,



- 714 Mason, K. E., Sheppard, L. J., Sverdrup, H., Haeuber, R., Hicks, W. K., Springer,
715 the Netherlands, 49–56, https://doi.org/10.1007/978-94-007-7939-6_6, 2014.
- 716 Feng, J., Vet, R., Cole, A., Zhang, L., Cheng, I., O'Brien, J., and Macdonald, A.-M.:
717 Inorganic chemical components in precipitation in the eastern U.S. and Eastern
718 Canada during 1989–2016: Temporal and regional trends of wet concentration and
719 wet deposition from the NADP and CAPMoN measurements, *Atmos. Environ.*,
720 254, 118367, <https://doi.org/10.1016/j.atmosenv.2021.118367>, 2021.
- 721 Fowler, D., Pyle, J. A., Raven, J. A., and Sutton, M. A.: The global nitrogen cycle in
722 the twenty-first century: introduction, *Philos. Trans. R. Soc.*, 368,
723 <https://doi.org/10.1098/rstb.2013.0165>, 2013.
- 724 Fu, B., Li, S., Yu, X., Yang, P., Yu, G., Feng, R., and Zhuang, X.: Chinese ecosystem
725 research network: Progress and perspectives, *Ecol. Complex.*, 7, 225-233,
726 <https://doi.org/10.1016/j.ecocom.2010.02.007>, 2010.
- 727 Fu, J. S., Carmichael, G. R., Dentener, F., Aas, W., Andersson, C., Barrie, L. A., Cole,
728 A., Galy-Lacaux, C., Geddes, J., Itahashi, S., Kanakidou, M., Labrador, L., Paulot,
729 F., Schwede, D., Tan, J., and Vet, R.: Improving Estimates of Sulfur, Nitrogen, and
730 Ozone Total Deposition through Multi-Model and Measurement-Model Fusion
731 Approaches, *Environ. Sci. Technol.*, <https://doi.org/10.1021/acs.est.1c05929>,
732 2022.
- 733 Holland, E. A., Braswell, B. H., Sulzman, J., and Lamarque, J. F.: Nitrogen deposition
734 onto the United States and Western Europe: synthesis of observations and models,
735 *Ecol. Appl.*, 15, 38-57, 2005.
- 736 Hou, Y., Wang, L., Zhou, Y., Wang, S., Liu, W., and Zhu, J.: Analysis of the
737 tropospheric column nitrogen dioxide over China based on satellite observations
738 during 2008–2017, *Atmos. Pollut. Res.*, 10, 651-655,
739 <https://doi.org/10.1016/j.apr.2018.11.003>, 2019.



- 740 Jia, Y., Yu, G., Gao, Y., He, N., Wang, Q., Jiao, C., and Zuo, Y.: Global inorganic
741 nitrogen dry deposition inferred from ground- and space-based measurements, *Sci*
742 *Rep*, 6, 19810, <https://doi.org/10.1038/srep19810>, 2016.
- 743 Kang, Y., Liu, M., Song, Y., Huang, X., Yao, H., Cai, X., Zhang, H., Kang, L., Liu, X.,
744 Yan, X., He, H., Zhang, Q., Shao, M., and Zhu, T.: High-resolution ammonia
745 emissions inventories in China from 1980 to 2012, *Atmos. Chem. Phys.*, 16,
746 2043-2058, <https://doi.org/10.5194/acp-16-2043-2016>, 2016.
- 747 Karplus, V. J., Zhang, S., and Almond, D.: Quantifying coal power plant responses to
748 tighter SO₂ emissions standards in China, *Proc. Natl. Acad. Sci.*, 115, 7004-7009,
749 <https://doi.org/10.1073/pnas.1800605115>, 2018.
- 750 Keller, C. A., Long, M. S., Yantosca, R. M., Da Silva, A. M., Pawson, S., and Jacob, D.
751 J.: HEMCO v1.0: a versatile, ESMF-compliant component for calculating
752 emissions in atmospheric models, *Geosci. Model Dev.*, 7, 1409-1417,
753 <https://doi.org/10.5194/gmd-7-1409-2014>, 2014.
- 754 Keresztesi, Á., Birsan, M.-V., Nita, I.-A., Bodor, Z., and Szép, R.: Assessing the
755 neutralisation, wet deposition and source contributions of the precipitation
756 chemistry over Europe during 2000–2017, *Environ. Sci. Eur.*, 31,
757 <https://doi.org/10.1186/s12302-019-0234-9>, 2019.
- 758 Krotkov, N.A., Lamsal, L.N., Marchenko, S.V., Celarier, E.A., J.Bucsela, E., Swartz,
759 W.H., Joiner, J., team, t.O.c.: OMI/Aura NO₂ Cloud-Screened Total and
760 Tropospheric Column L3 Global Gridded 0.25 degree × 0.25 degree V3. NASA
761 Goddard Space Flight Center, Goddard Earth Sciences Data and Information
762 Services Center (GES DISC).
763 <https://doi.org/10.5067/Aura/OMI/DATA/DATA3007>, 2019.
- 764 Krotkov, N. A., McLinden, C. A., Li, C., Lamsal, L. N., Celarier, E. A., Marchenko, S.
765 V., Swartz, W. H., Bucsela, E. J., Joiner, J., Duncan, B. N., Boersma, K. F.,
766 Veefkind, J. P., Levelt, P. F., Fioletov, V. E., Dickerson, R. R., He, H., Lu, Z., and
767 Streets, D. G.: Aura OMI observations of regional SO₂ and NO₂ pollution changes



- 768 from 2005 to 2015, *Atmos. Chem. Phys.*, 16, 4605-4629,
769 <https://doi.org/10.5194/acp-16-4605-2016>, 2016.
- 770 Kuhn, M.: caret: Classification and Regression Training. R package version 6.0-90.
771 <https://CRAN.R-project.org/package=caret>, 2021.
- 772 Li, J.: Pollution trends in China from 2000 to 2017: A multi-sensor view from space,
773 *Remote Sens.*, 12, 208, <https://doi.org/10.3390/rs12020208>, 2020.
- 774 Li, M., Klimont, Z., Zhang, Q., Martin, R. V., Zheng, B., Heyes, C., Cofala, J., Zhang,
775 Y., and He, K.: Comparison and evaluation of anthropogenic emissions of SO₂
776 and NO_x over China, *Atmos. Chem. Phys.*, 18, 3433-3456,
777 <https://doi.org/10.5194/acp-18-3433-2018>, 2018.
- 778 Li, M., Liu, H., Geng, G., Hong, C., Liu, F., Song, Y., Tong, D., Zheng, B., Cui, H.,
779 Man, H., Zhang, Q., and He, K.: Anthropogenic emission inventories in China: a
780 review, *Natl. Sci. Rev.*, 4, 834-866, <https://doi.org/10.1093/nsr/nwx150>, 2017.
- 781 Li, R., Cui, L., Meng, Y., Zhao, Y., and Fu, H.: Satellite-based prediction of daily SO₂
782 exposure across China using a high-quality random forest-spatiotemporal Kriging
783 (RF-STK) model for health risk assessment, *Atmos. Environ.*, 208, 10-19,
784 <https://doi.org/10.1016/j.atmosenv.2019.03.029>, 2019.
- 785 Li, R., Cui, L., Fu, H., Zhao, Y., Zhou, W., and Chen, J.: Satellite-Based Estimates of
786 Wet Ammonium (NH₄-N) Deposition Fluxes Across China during 2011-2016
787 Using a Space-Time Ensemble Model, *Environ. Sci. Technol.*, 54, 13419-13428,
788 <https://doi.org/10.1021/acs.est.0c03547>, 2020a.
- 789 Li, R., Cui, L., Liang, J., Zhao, Y., Zhang, Z., and Fu, H.: Estimating historical SO₂
790 level across the whole China during 1973-2014 using random forest model,
791 *Chemosphere*, 247, 125839, <https://doi.org/10.1016/j.chemosphere.2020.125839>,
792 2020b.
- 793 Li, Y., Schichtel, B. A., Walker, J. T., Schwede, D. B., Chen, X., Lehmann, C. M. B.,
794 Puchalski, M. A., Gay, D. A., and Collett, J. L., Jr.: Increasing importance of



- 795 deposition of reduced nitrogen in the United States, *Proc. Natl. Acad. Sci.*, 113,
796 5874-5879, <https://doi.org/10.1073/pnas.1525736113>, 2016.
- 797 Likens, G. E., Butler, T. J., Claybrooke, R., Vermeylen, F., and Larson, R.: Long-term
798 monitoring of precipitation chemistry in the U.S.: Insights into changes and
799 condition, *Atmos. Environ.*, 245, 118031,
800 <https://doi.org/10.1016/j.atmosenv.2020.118031>, 2021.
- 801 Liu, F., Zhang, Q., Tong, D., Zheng, B., Li, M., Huo, H., and He, K. B.:
802 High-resolution inventory of technologies, activities, and emissions of coal-fired
803 power plants in China from 1990 to 2010, *Atmos. Chem. Phys.*, 15, 13299-13317,
804 <https://doi.org/10.5194/acp-15-13299-2015>, 2015.
- 805 Liu, L., Zhang, X., Xu, W., Liu, X., Lu, X., Wang, S., Zhang, W., and Zhao, L.: Ground
806 Ammonia Concentrations over China Derived from Satellite and Atmospheric
807 Transport Modeling, *Remote Sens.*, 9, 467, <https://doi.org/10.3390/rs9050467>,
808 2017a.
- 809 Liu, L., Zhang, X., Xu, W., Liu, X., Lu, X., Chen, D., Zhang, X., Wang, S., and Zhang,
810 W.: Estimation of monthly bulk nitrate deposition in China based on satellite NO₂
811 measurement by the Ozone Monitoring Instrument, *Remote Sens. Environ.*, 199,
812 93-106, <https://doi.org/10.1016/j.rse.2017.07.005>, 2017b.
- 813 Liu, L., Xu, W., Lu, X., Zhong, B., Guo, Y., Lu, X., Zhao, Y., He, W., Wang, S., Zhang,
814 X., Liu, X., and Vitousek, P.: Exploring global changes in agricultural ammonia
815 emissions and their contribution to nitrogen deposition since 1980, *Proc. Natl.*
816 *Acad. Sci.*, 119, e2121998119, <https://doi.org/10.1073/pnas.2121998119>, 2022.
- 817 Liu, M., Huang, X., Song, Y., Xu, T., Wang, S., Wu, Z., Hu, M., Zhang, L., Zhang, Q.,
818 Pan, Y., Liu, X., and Zhu, T.: Rapid SO₂ emission reductions significantly increase
819 tropospheric ammonia concentrations over the North China Plain, *Atmos. Chem.*
820 *Phys.*, 18, 17933-17943, <https://doi.org/10.5194/acp-18-17933-2018>, 2018.
- 821 Liu, M. Y., Lin, J. T., Boersma, K. F., Pinaridi, G., Wang, Y., Chimot, J., Wagner, T., Xie,
822 P. H., Eskes, H., Van Roozendaal, M., Hendrick, F., Wang, P. C., Wang, T., Yan, Y.



- 823 Y., Chen, L. L., and Ni, R. J.: Improved aerosol correction for OMI tropospheric
824 NO₂ retrieval over East Asia: constraint from CALIOP aerosol vertical profile,
825 Natl. Sci. Rev, 12, 1-21, <https://doi.org/10.5194/amt-12-1-2019>, 2019.
- 826 Liu, X.J., Zhang, Y., Han, W.X., Tang, A.H., Shen, J.L., Cui, Z.L., Vitousek, P.,
827 Erisman, J.W., Goulding, K., Christie, P., Fangmeier, A., and Zhang, F.S.:
828 Enhanced nitrogen deposition over China. Nature 494, 459-462,
829 <https://doi.org/10.1038/nature11917>, 2013.
- 830 Liu, X. J., Xu, W., Du, E. Z., Tang, A. H., Zhang, Y., Wen, Z., Hao, T. X., Pan, Y. P.,
831 Zhang, L., Zhao, Y., Shen, J. L., Zhou, F., Gao, Z. L., Chang, Y. H., Goulding, K.,
832 Collett, J. L., Jr., Vitousek, P. M., Zhang, F. S., Zhang, Y. Y., Gu, B. J., and Feng,
833 Z. Z.: Environmental impacts of nitrogen emissions in China and the role of
834 policies in emission reduction, Philos. Trans. Royal Soc., 378,
835 <https://doi.org/10.1098/rsta.2019.0324>, 2020.
- 836 Lu, X., Ye, X., Zhou, M., Zhao, Y., Weng, H., Kong, H., Li, K., Gao, M., Zheng, B.,
837 Lin, J., Zhou, F., Zhang, Q., Wu, D., Zhang, L., and Zhang, Y.: The
838 underappreciated role of agricultural soil nitrogen oxide emissions in ozone
839 pollution regulation in North China, Nat. Commun., 12, 5021,
840 <https://doi.org/10.1038/s41467-021-25147-9>, 2021.
- 841 Luo, X., Pan, Y., Goulding, K., Zhang, L., Liu, X., and Zhang, F.: Spatial and seasonal
842 variations of atmospheric sulfur concentrations and dry deposition at 16 rural and
843 suburban sites in China, Atmos. Environ., 146, 79-89,
844 <https://doi.org/10.1016/j.atmosenv.2016.07.038>, 2016.
- 845 Lye, C. and Tian, H.: Spatial and temporal patterns of nitrogen deposition in China:
846 Synthesis of observational data, J. Geophys. Res., 112,
847 <https://doi.org/10.1029/2006jd007990>, 2007.
- 848 Pan, Y. P., Wang, Y. S., Tang, G. Q., and Wu, D.: Wet and dry deposition of
849 atmospheric nitrogen at ten sites in Northern China, Atmos. Chem. Phys., 12,
850 6515-6535, <https://doi.org/10.5194/acp-12-6515-2012>, 2012.



- 851 Payne, R. J., Stevens, C. J., Dise, N. B., Gowing, D. J., Pilkington, M. G., Phoenix, G.
852 K., Emmett, B. A., and Ashmore, M. R.: Impacts of atmospheric pollution on the
853 plant communities of British acid grasslands, *Environ. Pollut.*, 159, 2602-2608,
854 <https://doi.org/10.1016/j.envpol.2011.06.009>, 2011.
- 855 Qin, K., Han, X., Li, D., Xu, J., Loyola, D., Xue, Y., Zhou, X., Li, D., Zhang, K., and
856 Yuan, L.: Satellite-based estimation of surface NO₂ concentrations over
857 east-central China: A comparison of POMINO and OMNO2d data, *Atmos.*
858 *Environ.*, 224, 117322, <https://doi.org/10.1016/j.atmosenv.2020.117322>, 2020.
- 859 Reuss, J. O., Cosby, B. J., and Wright, R. F.: Chemical processes governing soil and
860 water acidification, *Nature*, 329, 27-32, <https://www.nature.com/articles/329027a0>,
861 1987.
- 862 Simpson, D., Benedictow, A., Berge, H., Bergström, R., Emberson, L. D., Fagerli, H.,
863 Flechard, C. R., Hayman, G. D., Gauss, M., Jonson, J. E., Jenkin, M. E., Nyíri, A.,
864 Richter, C., Semeena, V. S., Tsyro, S., Tuovinen, J. P., Valdebenito, Á., and Wind,
865 P.: The EMEP MSC-W chemical transport model – technical description, *Atmos.*
866 *Chem. Phys.*, 12, 7825-7865, <https://doi.org/10.5194/acp-12-7825-2012>, 2012.
- 867 Theobald, M. R., Vivanco, M. G., Aas, W., Andersson, C., Ciarelli, G., Couvidat, F.,
868 Cuvelier, K., Manders, A., Mircea, M., Pay, M.-T., Tsyro, S., Adani, M.,
869 Bergström, R., Bessagnet, B., Briganti, G., Cappelletti, A., amp, apos, Isidoro, M.,
870 Fagerli, H., Mar, K., Otero, N., Raffort, V., Roustan, Y., Schaap, M., Wind, P., and
871 Colette, A.: An evaluation of European nitrogen and sulfur wet deposition and
872 their trends estimated by six chemistry transport models for the period 1990–2010,
873 *Atmos. Chem. Phys.*, 19, 379-405, <https://doi.org/10.5194/acp-19-379-2019>,
874 2019.
- 875 Tørseth, K., Aas, W., Breivik, K., Fjæraa, A. M., Fiebig, M., Hjellbrekke, A. G., Lund
876 Myhre, C., Solberg, S., and Yttri, K. E.: Introduction to the European Monitoring
877 and Evaluation Programme (EMEP) and observed atmospheric composition



- 878 change during 1972–2009, *Atmos. Chem. Phys.*, 12, 5447-5481,
879 <https://doi.org/10.5194/acp-12-5447-2012>, 2012.
- 880 Totsuka, T., Sase, H., and Shimizu, H.: Major activities of acid deposition monitoring
881 network in East Asia (EANET) and related studies. In: *Plant responses to air
882 pollution and global change*. Springer, pp. 251-259, 2005.
- 883 Vet, R., Artz, R. S., Carou, S., Shaw, M., Ro, C.-U., Aas, W., Baker, A., Bowersox, V.
884 C., Dentener, F., Galy-Lacaux, C., Hou, A., Pienaar, J. J., Gillett, R., Forti, M. C.,
885 Gromov, S., Hara, H., Khodzher, T., Mahowald, N. M., Nickovic, S., Rao, P. S. P.,
886 and Reid, N. W.: A global assessment of precipitation chemistry and deposition of
887 sulfur, nitrogen, sea salt, base cations, organic acids, acidity and pH, and
888 phosphorus, *Atmos. Environ.*, 93, 3-100,
889 <https://doi.org/10.1016/j.atmosenv.2013.10.060>, 2014.
- 890 Wang, J., Sha, Z., Zhang, J., Kang, J., Xu, W., Goulding, K., and Liu, X.: Reactive N
891 emissions from cropland and their mitigation in the North China Plain, *Environ.
892 Res.*, 214, 114015, <https://doi.org/10.1016/j.envres.2022.114015>, 2022.
- 893 Wen, Z., Xu, W., Li, Q.Q., Han, M.J., Tang, A.H., Zhang, Y., Luo, X.S., Shen, J.L.,
894 Wang, W., Li, K.H., Pan, Y.P., Zhang, L., Li, W.Q., Collett Jr, J.L., Zhong, B.Q.,
895 Wang, X.M., Goulding, K., Zhang, F.S., and Liu, X.J.: Changes of nitrogen
896 deposition in China from 1980 to 2018. *Environment International* 144, 106022,
897 <https://doi.org/10.1016/j.envint.2020.106022>, 2020.
- 898 Wesely, M. L.: Parameterization of surface resistances to gaseous dry deposition in
899 regional-scale numerical models, *Atmos. Environ.*, 23, 1293-1304,
900 [https://doi.org/https://doi.org/10.1016/0004-6981\(89\)90153-4](https://doi.org/https://doi.org/10.1016/0004-6981(89)90153-4), 1989.
- 901 Whitburn, S., Van Damme, M., Clarisse, L., Bauduin, S., Heald, C. L., Hadji-Lazaro, J.,
902 Hurtmans, D., Zondlo, M. A., Clerbaux, C., and Coheur, P. F.: A flexible and
903 robust neural network IASI-NH₃ retrieval algorithm, *Journal of Geophysical
904 Research: Atmospheres*, 121, 6581-6599, <https://doi.org/10.1002/2016jd024828>,
905 2016.



- 906 Wu, Y., Di, B., Luo, Y., Grieneisen, M. L., Zeng, W., Zhang, S., Deng, X., Tang, Y., Shi,
907 G., Yang, F., and Zhan, Y.: A robust approach to deriving long-term daily surface
908 NO₂ levels across China: Correction to substantial estimation bias in
909 back-extrapolation, *Environ. Int.*, 154, 106576,
910 <https://doi.org/10.1016/j.envint.2021.106576>, 2021.
- 911 Xia, Y., Zhao, Y., and Nielsen, C. P.: Benefits of China's efforts in gaseous pollutant
912 control indicated by the bottom-up emissions and satellite observations 2000–
913 2014, *Atmos. Environ.*, 136, 43-53,
914 <https://doi.org/10.1016/j.atmosenv.2016.04.013>, 2016.
- 915 Xu, W., Zhang, L., and Liu, X.: A database of atmospheric nitrogen concentration and
916 deposition from the nationwide monitoring network in China, *Sci. Data*, 6, 51,
917 <https://doi.org/10.1038/s41597-019-0061-2>, 2019.
- 918 Xu, W., Liu, L., Cheng, M., Zhao, Y., Zhang, L., Pan, Y., Zhang, X., Gu, B., Li, Y.,
919 Zhang, X., Shen, J., Lu, L., Luo, X., Zhao, Y., Feng, Z., Collett Jr, J. L., Zhang, F.,
920 and Liu, X.: Spatial-temporal patterns of inorganic nitrogen air concentrations
921 and deposition in eastern China, *Atmos. Chem. Phys.*, 18, 10931-10954,
922 <https://doi.org/10.5194/acp-18-10931-2018>, 2018.
- 923 Xu, W., Luo, X. S., Pan, Y. P., Zhang, L., Tang, A. H., Shen, J. L., Zhang, Y., Li, K. H.,
924 Wu, Q. H., Yang, D. W., Zhang, Y. Y., Xue, J., Li, W. Q., Li, Q. Q., Tang, L., Lu, S.
925 H., Liang, T., Tong, Y. A., Liu, P., Zhang, Q., Xiong, Z. Q., Shi, X. J., Wu, L. H.,
926 Shi, W. Q., Tian, K., Zhong, X. H., Shi, K., Tang, Q. Y., Zhang, L. J., Huang, J. L.,
927 He, C. E., Kuang, F. H., Zhu, B., Liu, H., Jin, X., Xin, Y. J., Shi, X. K., Du, E. Z.,
928 Dore, A. J., Tang, S., Collett, J. L., Goulding, K., Sun, Y. X., Ren, J., Zhang, F. S.,
929 and Liu, X. J.: Quantifying atmospheric nitrogen deposition through a nationwide
930 monitoring network across China, *Atmos. Chem. Phys.*, 15, 12345-12360,
931 <https://doi.org/10.5194/acp-15-12345-2015>, 2015.



- 932 Xu, X.: China's GDP and POP spatial distribution kilometer grid dataset. Resources
933 and environment science data registration and publication system
934 (<http://www.resdc.cn/DOI>), 2017.
- 935 Yamaga, S., Ban, S., Xu, M., Sakurai, T., Itahashi, S., and Matsuda, K.: Trends of
936 sulfur and nitrogen deposition from 2003 to 2017 in Japanese remote areas,
937 Environ. Pollut., 289, 117842, <https://doi.org/10.1016/j.envpol.2021.117842>,
938 2021.
- 939 Yu, G., Jia, Y., He, N., Zhu, J., Chen, Z., Wang, Q., Piao, S., Liu, X., He, H., Guo, X.,
940 Wen, Z., Li, P., Ding, G., and Goulding, K.: Stabilization of atmospheric nitrogen
941 deposition in China over the past decade, Nature Geosci., 12, 424-431,
942 <https://doi.org/10.1038/s41561-019-0352-4>, 2019.
- 943 Zhan, X., Yu, G., He, N., Jia, B., Zhou, M., Wang, C., Zhang, J., Zhao, G., Wang, S.,
944 Liu, Y., and Yan, J.: Inorganic nitrogen wet deposition: Evidence from the
945 North-South Transect of Eastern China, Environ. Pollut., 204, 1-8,
946 <https://doi.org/10.1016/j.envpol.2015.03.016>, 2015.
- 947 Zhang, G., Pan, Y., Tian, S., Cheng, M., Xie, Y., Wang, H., and Wang, Y.: Limitations
948 of passive sampling technique of rainfall chemistry and wet deposition flux
949 characterization, Res. Environ., 28, 684-690, 2015.
- 950 Zhang, Q., Zheng, Y., Tong, D., Shao, M., Wang, S., Zhang, Y., Xu, X., Wang, J., He,
951 H., Liu, W., Ding, Y., Lei, Y., Li, J., Wang, Z., Zhang, X., Wang, Y., Cheng, J., Liu,
952 Y., Shi, Q., Yan, L., Geng, G., Hong, C., Li, M., Liu, F., Zheng, B., Cao, J., Ding,
953 A., Gao, J., Fu, Q., Huo, J., Liu, B., Liu, Z., Yang, F., He, K., and Hao, J.: Drivers
954 of improved PM_{2.5} air quality in China from 2013 to 2017, Proc. Natl. Acad. Sci.,
955 116, 24463-24469, <https://doi.org/10.1073/pnas.1907956116>, 2019.
- 956 Zhang, T., Chen, H. Y. H., and Ruan, H.: Global negative effects of nitrogen deposition
957 on soil microbes, ISME J, 12, 1817-1825,
958 <https://doi.org/10.1038/s41396-018-0096-y>, 2018a.



- 959 Zhang, X. Y., Chuai, X. W., Liu, L., Zhang, W. T., Lu, X. H., Zhao, L. M., and Chen, D.
960 M.: Decadal trends in wet sulfur deposition in China estimated from OMI SO₂
961 columns, *J. Geophys. Res. (Atmos.)*, 123, 10796-10811,
962 <https://doi.org/10.1029/2018jd028770>, 2018b.
- 963 Zhang, Y., Liu, X. J., Fangmeier, A., Goulding, K. T. W., and Zhang, F. S.: Nitrogen
964 inputs and isotopes in precipitation in the North China Plain, *Atmos. Environ.*, 42,
965 1436-1448, <https://doi.org/10.1016/j.atmosenv.2007.11.002>, 2008.
- 966 Zhang, Y., Wang, T. J., Hu, Z. Y., and Xu, C. K.: Temporal variety and spatial
967 distribution of dry deposition velocities of typical air pollutants over different
968 land-use types, *Climatic Environ. Res.*, 9, 591-604, 2004. (in Chinese)
- 969 Zhang, Y., Zhao, J., and Yin, H.: European Union agricultural policy transformation
970 trend and enlightenment, *World Agriculture*, 05, 2020. (in Chinese)
- 971 Zhao, Y., Xi, M., Zhang, Q., Dong, Z., Ma, M., Zhou, K., Xu, W., Xing, J., Zheng, B.,
972 Wen, Z., Liu, X., Nielsen, C. P., Liu, Y., Pan, Y., and Zhang, L.: Decline in bulk
973 deposition of air pollutants in China lags behind reductions in emissions, *Nature*
974 *Geosci.*, 15, 190-195, <https://doi.org/10.1038/s41561-022-00899-1>, 2022.
- 975 Zheng, B., Tong, D., Li, M., Liu, F., Hong, C., Geng, G., Li, H., Li, X., Peng, L., Qi, J.,
976 Yan, L., Zhang, Y., Zhao, H., Zheng, Y., He, K., and Zhang, Q.: Trends in China's
977 anthropogenic emissions since 2010 as the consequence of clean air actions,
978 *Atmos. Chem. Phys.*, 18, 14095-14111,
979 <https://doi.org/10.5194/acp-18-14095-2018>, 2018a.
- 980 Zheng, X. D., Liu, X. Y., Song, W., Sun, X. C., and Liu, C. Q.: Nitrogen isotope
981 variations of ammonium across rain events: Implications for different scavenging
982 between ammonia and particulate ammonium, *Environ. Pollut.*, 239, 392-398,
983 <https://doi.org/10.1016/j.envpol.2018.04.015>, 2018b.
- 984 Zhou, K., Zhao, Y., Zhang, L., and Xi, M.: Declining dry deposition of NO₂ and SO₂
985 with diverse spatiotemporal patterns in China from 2013 to 2018, *Atmos. Environ.*,
986 262, 118655, <https://doi.org/10.1016/j.atmosenv.2021.118655>, 2021.



987 Zhu, J., He, N., Wang, Q., Yuan, G., Wen, D., Yu, G., and Jia, Y.: The composition,
988 spatial patterns, and influencing factors of atmospheric wet nitrogen deposition in
989 Chinese terrestrial ecosystems, *Sci. Total Environ.*, 511, 777-785,
990 <https://doi.org/10.1016/j.scitotenv.2014.12.038>, 2015.
991



992 **Figure captions**

993 Figure 1 The research domain of this study. The pink points represent CNEMC and the
994 green points represent NNDMN. The Qinling-Huaihe Line is the boundary between the
995 north and the south of the country.

996 Figure 2 Methodology framework to estimate dry and wet deposition of this study. The
997 blue process shows the four steps to establish the RF model. The orange process shows
998 the three steps in establishing a GAM model. See Sections 2.2 to 2.3 of the method
999 section in the text for the acquisition of the preliminary data set.

1000 Figure 3 Comparison of deposition between this study and other literatures for dry (a),
1001 wet (b) and total deposition (c). The black cross and the pentagram are the average of
1002 literature-reported results and the multi-year average of this study, respectively. The
1003 boxplots represent the dispersion of deposition collected from literatures. The central
1004 horizontal line, the upper side line, and the lower side line of the box represent the
1005 median value, the upper quartile (75th Quantile, Q3) and the lower quartile (25th
1006 Quantile, Q1). The vertical line extending out of the box represents 1.5 times the
1007 interquartile interval (IQR, i.e., Q3-Q1), and the horizontal lines represent the upper
1008 limit (Q3+1.5IQR) and the lower limit (Q1-1.5 IQR).

1009 Figure 4 Contribution of different forms and species to the estimated total N and S
1010 deposition in China.

1011 Figure 5 The interannual variability of N and S deposition, emissions and component
1012 proportion in China from 2005 to 2020. The emission data over China were taken from
1013 MEIC.

1014 Figure 6 The interannual variations of emissions, deposition and RDN/OXN for China,
1015 28 Europe countries (EU) and the USA. All the data are relative to the 2005 levels. The
1016 grey dotted lines are a visual guidance for 1.0 on each of the y axes. (a) NO_x emissions
1017 and OXN deposition; (b) NH₃ emissions and RDN deposition; (c) SO₂ emissions and
1018 sulfur deposition; and (d) RDN/OXN.

1019 Figure 7 The spatial distributions of N and S deposition flux in 2005-2020.

1020 Figure 8 The interannual variations and relative changes of deposition of OXN (a),
1021 RDN (b) and sulfur (c) by region. All the data are relative to the 2005 levels. The



1022 orange line represents eastern China (SE+NC with Inner Mongolia excluded, see
1023 Figure 1 for the region definitions), the blue line represents western China (NW+TP),
1024 and the red line represents the average level of whole China.

1025 Figure 9 Annual mean D/E ratio of OXN, RDN and sulfur from 2005 to 2020 in
1026 different regions (a) and linear relationship between regional deposition and emissions
1027 (b-d).

1028 Figure 10 The spatial distribution of multi-year seasonal variation of the total
1029 deposition across 2005-2020.

1030



1031 **Tables**

1032 **Table 1 Comparison of relative change rates of emissions and deposition in the**
 1033 **process of pollution control in China, Europe and the USA.** The starting and ending
 1034 time was selected according to the period of the fastest decline of deposition in China,
 1035 and the time period of emission decline was selected according to the reference
 1036 deposition. The emission data were respectively taken from MEIC, the European
 1037 Environment Agency (EEA, <https://www.eea.europa.eu/themes/air>), and U.S.
 1038 Environmental Protection Agency (EPA,
 1039 <https://www.epa.gov/air-emissions-inventories/air-pollutant-emissionstrends-data>,
 1040 while deposition data from European Monitoring and Evaluation Programme (EMEP,
 1041 <https://projects.nilu.no/ccc/index.html>) for Europe and Clean Air Status and Trends
 1042 Network (CASTNET, <https://www.epa.gov/castnet>) and National Atmospheric
 1043 Deposition Program (NADP,
 1044 <https://nadp.slh.wisc.edu/networks/national-trends-network/>) for the USA.

Relative change	Emissions			
		NO _x		SO ₂
The USA	-35.9%	(2003-2011)	-78.4%	(2003-2016)
Europe	-17.3%	(2000-2008)	-57.6%	(2000-2013)
China	-32.2%	(2012-2020)	-75.5%	(2007-2020)
Deposition				
	OXN		S	
The USA	-26.0%	(2003-2011)	-72.5%	(2003-2016)
Europe	-11.1%	(2000-2008)	-49.9%	(2000-2013)
China	-7.1%	(2012-2020)	-27.0%	(2007-2020)

1045



1046 **Table 2 The interannual changes in deposition and emissions of N and S by**
 1047 **regions for 2005–2020.** Eastern China includes NC (Inner Mongolia excluded) and SE,
 1048 and western China includes TP and NW (see Figure 1 for the region definitions). P1
 1049 and P2 indicate 2005–2012 and 2012–2020, respectively.

Interannual change (units: kg N/S ha ⁻¹ yr ⁻¹)		Whole China		Eastern China		Western China	
		P1	P2	P1	P2	P1	P2
Emissions	NO _x	0.60	-0.42	1.12	-1.33	0.63	-0.24
	NH ₃	0.08	-0.21	0.08	-0.83	0.09	-0.02
	SO ₂	-0.39	-1.24	-2.98	-4.62	0.01	-0.89
Deposition	Total OXN	0.09	-0.15	0.22	-0.41	0.07	-0.08
	Total RDN	0.05	0.06	0.06	0.28	0.05	0.22
	Total N	0.14	-0.09	0.28	-0.14	0.13	0.14
	Total S	-0.29	-0.82	-0.34	-1.55	-0.29	-0.60
Relative annual change to 2005 (P1) or 2012 (P2)		P1	P2	P1	P2	P1	P2
Emissions	NO _x	49%	-31%	17%	-25%	110%	-29%
	NH ₃	7%	-15%	2%	-22%	17%	-3%
	SO ₂	-13%	-72%	-25%	-73%	10%	-74%
Deposition	Total OXN	5%	-7%	9%	-12%	4%	-5%
	Total RDN	3%	3%	5%	9%	3%	10%
	Total N	4%	-2%	7%	-2%	3%	1%
	Total S	-7%	-21%	-3%	-28%	-9%	-18%

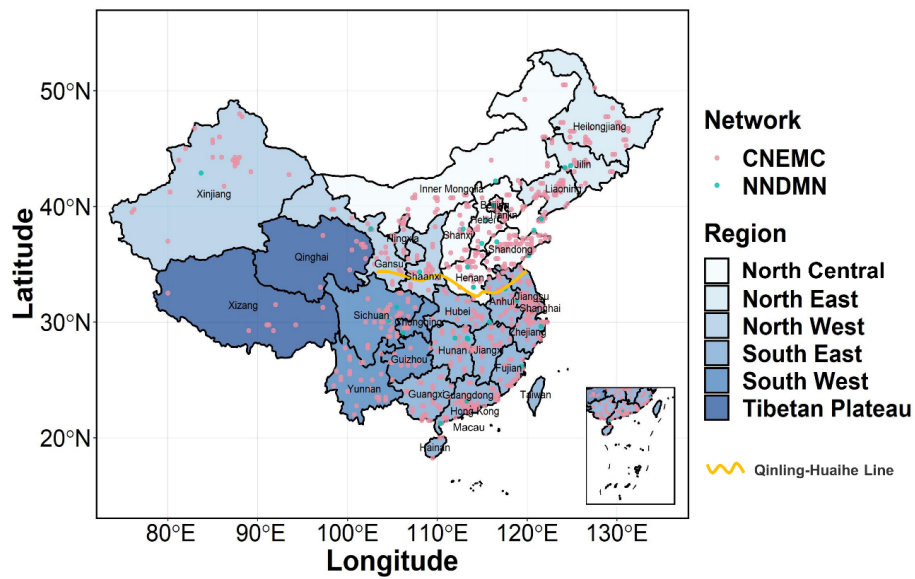
1050

1051



1052 **Figures**

1053 **Figure 1**

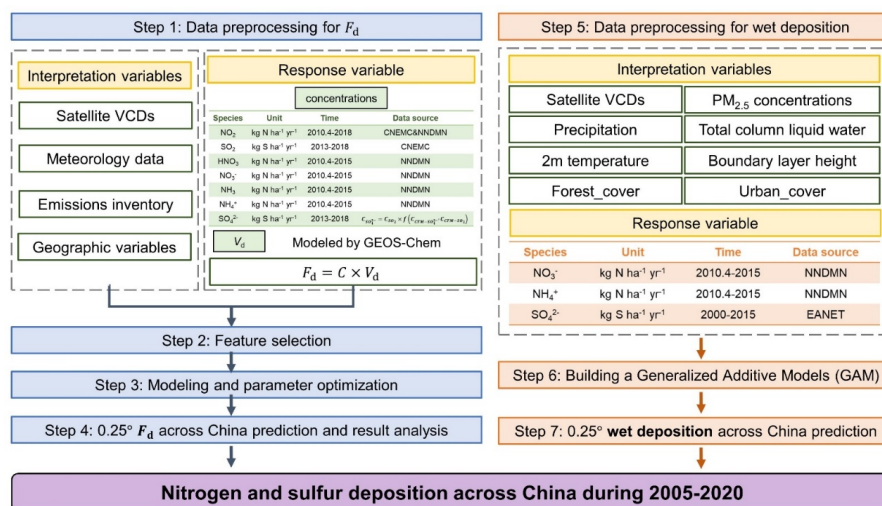


1054

1055



1056 **Figure 2**

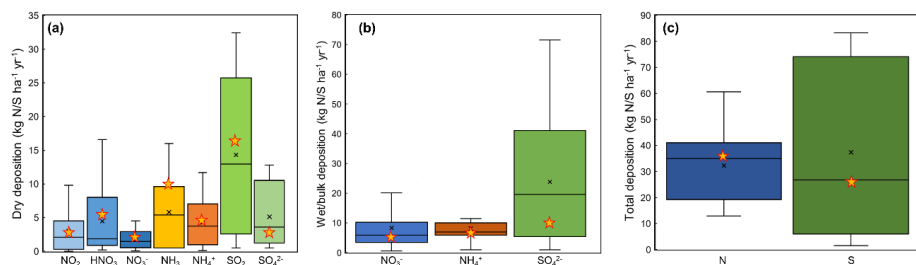


1057

1058



1059 **Figure 3**

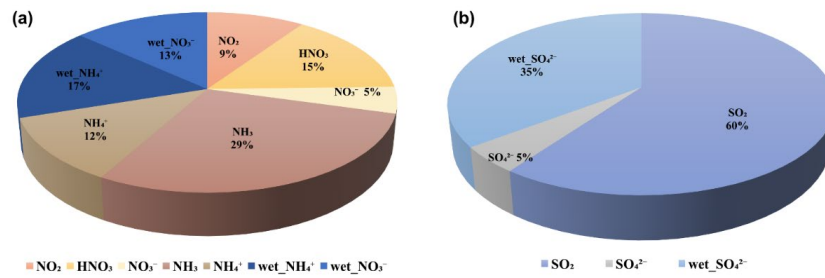


1060

1061



1062 **Figure 4**

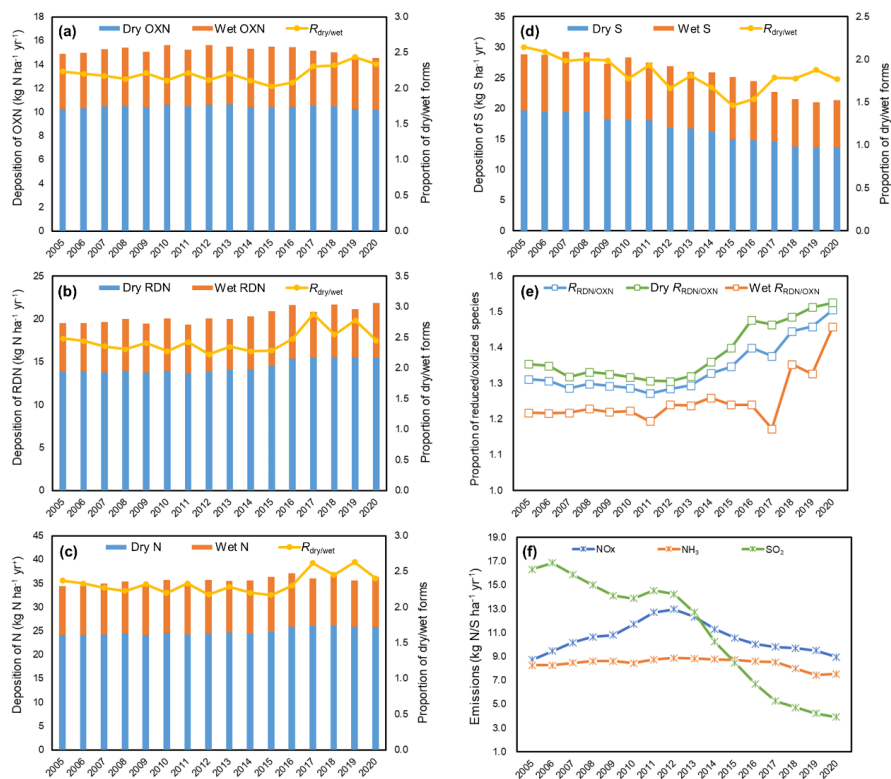


1063

1064



1065 **Figure 5**

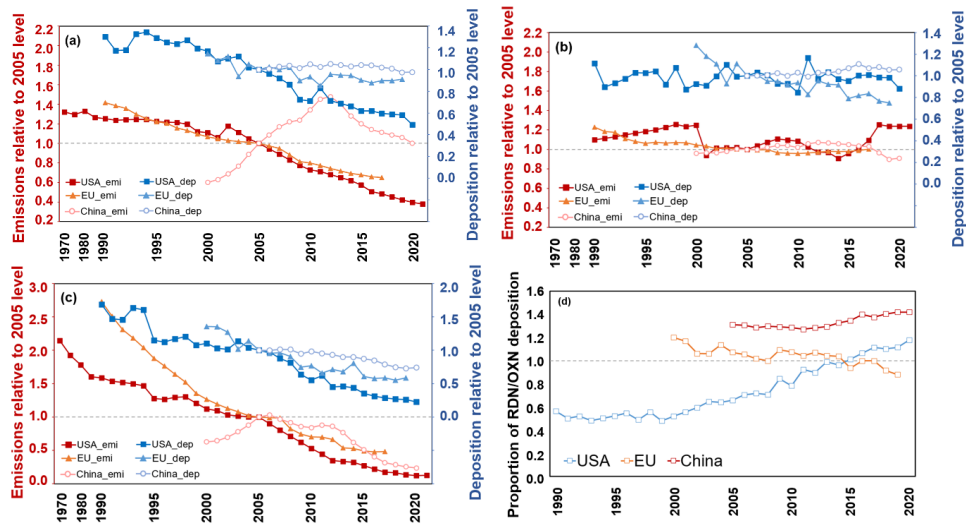


1066

1067



1068 **Figure 6**

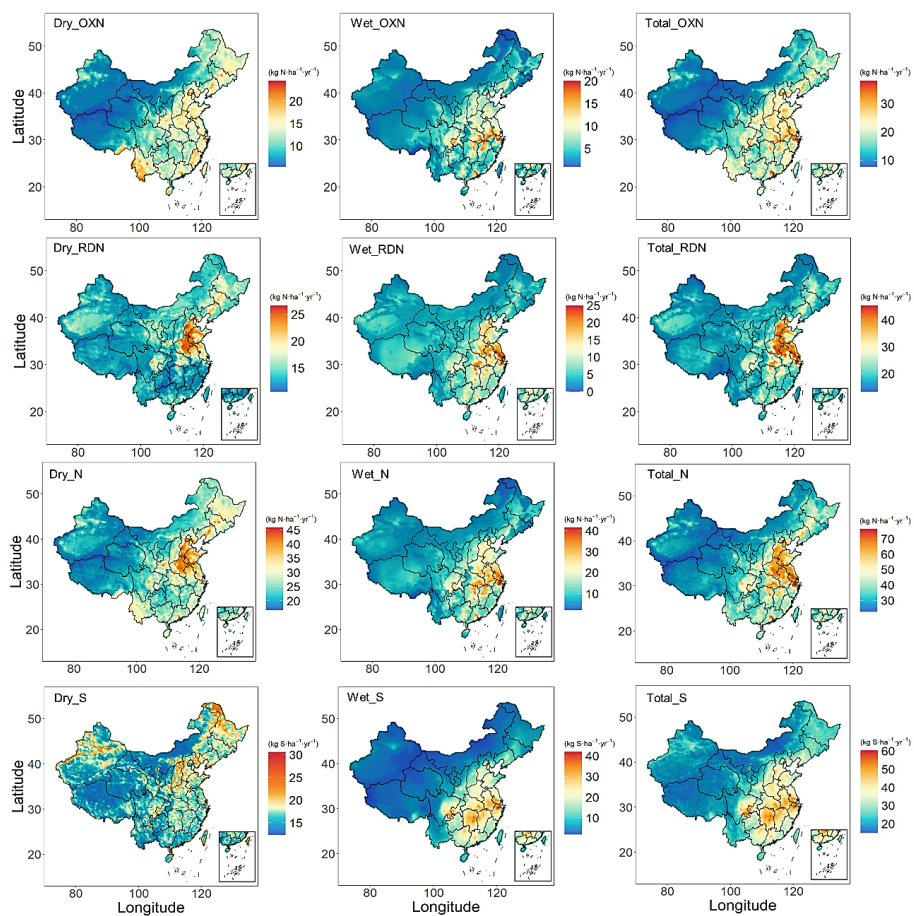


1069

1070



1071 **Figure 7**

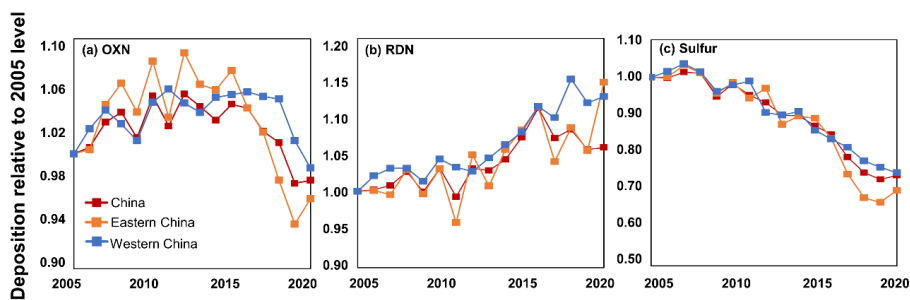


1072

1073



1074 **Figure 8**

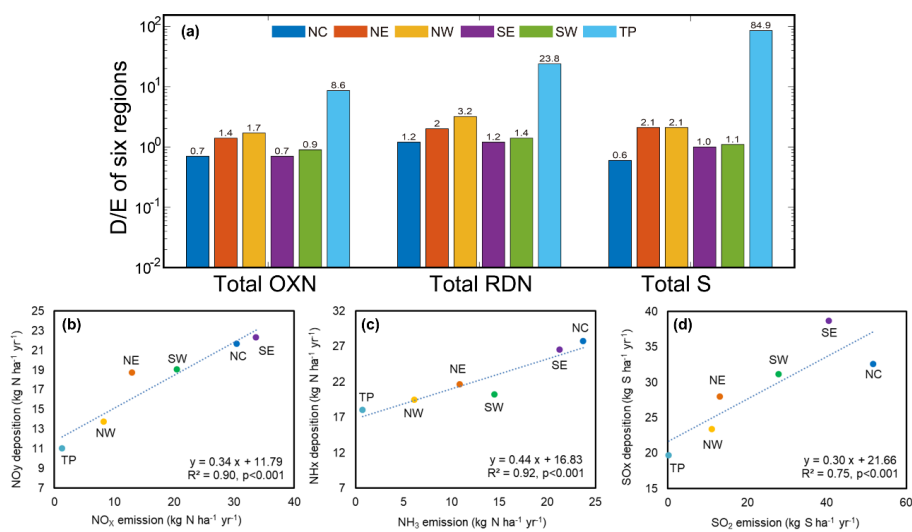


1075

1076



1077 **Figure 9**

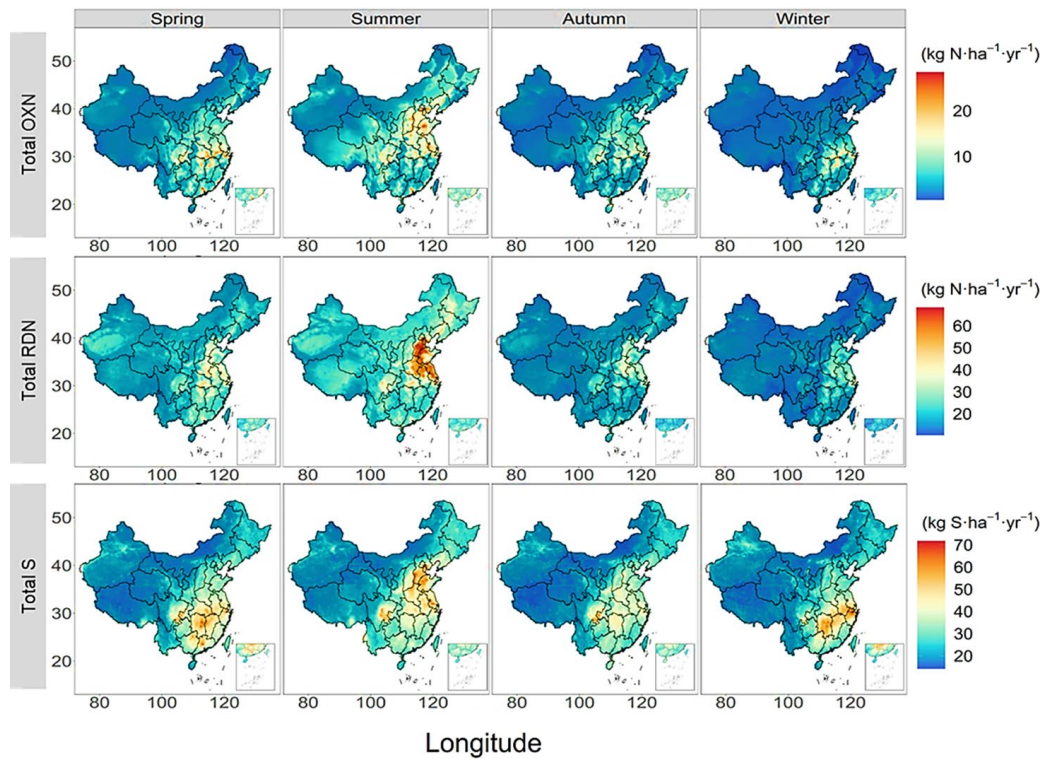


1078

1079



1080 **Figure 10**



1081

1082